ISTITUTO NAZIONALE DI FISICA NUCLEARE

Sezione di Genova

INFN/BE-89/6
27 Novembre 1989

G.P. Capitani, L. Casano, A.R. Reolon, M. Sanzone, A. Zucchiatti:

PHOTON SCATTERING FROM PROTON IN THE Δ REGION

Servizio Documentazione
dei Laboratori Nazionali di Frascati

INFN - Istituto Nazionale di Fisica Nucleare
Sezione di Genova

INFN/BE-89/6
27 Novembre 1989

PHOTON SCATTERING FROM PROTON IN THE Δ REGION

G.P.Capitani*, L.Casano*, A.R.Reolon*, M.Sanzone°, A.Zucchiatti°

* Istituto Nazionale di Fisica Nucleare - Laboratori Nazionali di Frascati I-00044 Frascati
° Dipartimento di Fisica dell'Universita' di Genova and Istituto Nazionale di Fisica Nucleare - Sezione di Genova I-16146 Genova

ABSTRACT: Precise measurements of the differential cross section for the photon scattering from proton are needed in order to study the role of nucleonic and non-nucleonic degrees of freedom in the elastic photoscattering process. The theoretical and experimental situation concerning the process is discussed. An experimental arrangement and a complex apparatus are planned which should allow measurements having a 2% statistical accuracy and a comparable systematic error. Detailed calculations of kinematics and a Monte-Carlo simulation of the experimental conditions are reported.

1. INTRODUCTION

Elastic photon scattering off nuclei as a pure electromagnetic process is a very interesting tool for the study of the internal structure of the system because the interaction is well known, because the photon is a weak probe able to penetrate into and explore the whole nucleus, and because no initial or final state distortion or other problems, connected with hadron reactions and with particle emission processes are involved. Moreover since the residual nucleus is left in its ground state, the theoretical interpretation is made simple because the ground-state properties of a nucleus are usually well known. Since the reaction proceeds in general via a two-step process, the whole internal dynamics of the system is participating in the intermediate state of the system.

As a consequence elastic photon scattering off the nucleus is considered one of the most promising processes in order to study nucleonic and non-nucleonic degrees of freedom in nuclei.

Experimentally it has been investigated at low energy by various groups and a few experiments exist above the Giant Dipole Resonance.

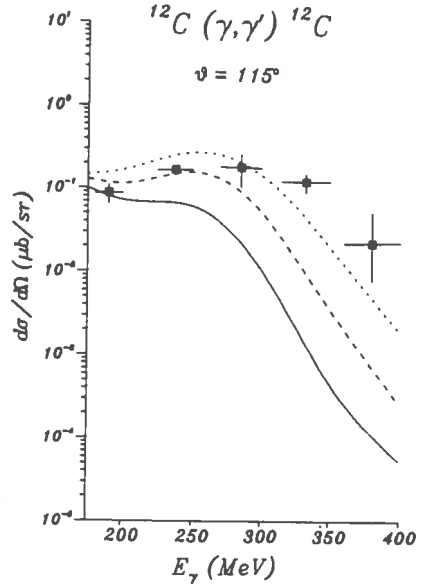

Fig.1 Differential cross section for the photon scattering from ^{12}C. Comparison between the experimental data of ref.2 a) and the calculations of ref.3

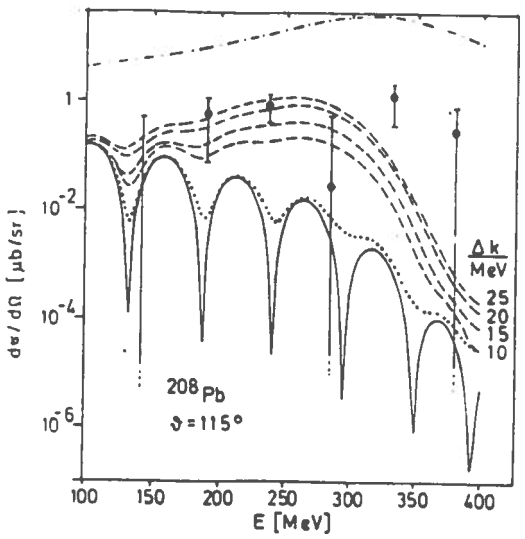

Fig.2 Differential cross section for the photon scattering from ^{208}Pb. Comparison between the experimental data of ref.2 a) and the calculations of ref.5

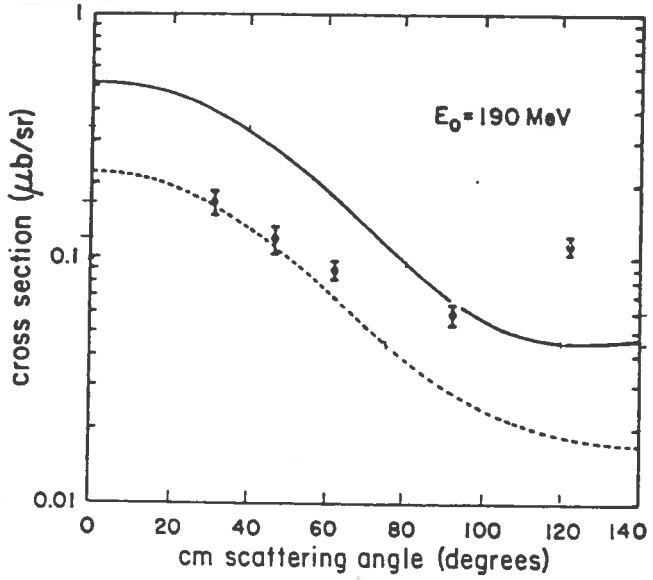

Fig.3 Differential cross section for the photon scattering from ^{4}He. Comparison between the experimental data at E = 190 MeV of ref.2 b) and the calculations of ref.4a and 4b

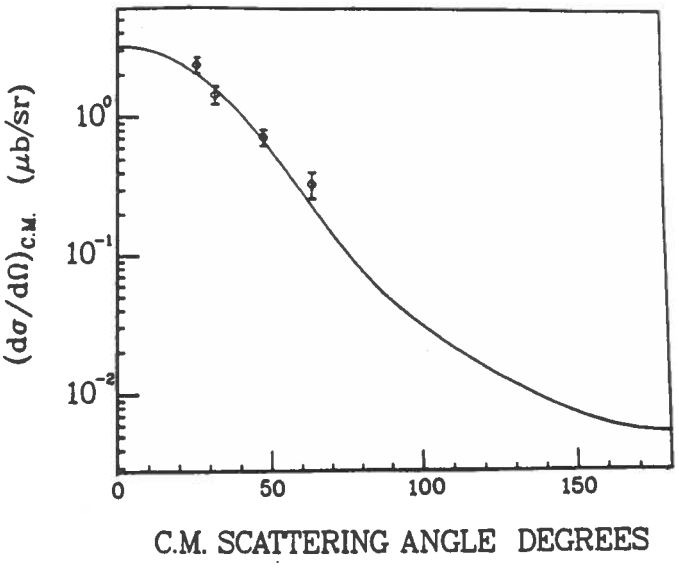

Fig.4 Differential cross section for the photon scattering from ^{4}He. Comparison between the experimental data at E = 320 MeV of ref.2 b) and the calculations of ref.4a and 4b

Below the pion production threshold the existing data[1] have clearly demonstrated the high sensitivity of the process to the proton and virtual pion-exchange spatial distributions.

At energies above the pion threshold only a few experimental data exist[2] mainly because of the difficulty of the experiment, arising from the competing process of π^o photoproduction decaying into photons and thus leading to photon-nucleus final states.

The general use of bremsstrahlung photon beams and the finite energy resolution of the apparatus make it very hard to separate the background contribution of photons from π^o decay and the inelastic photon scattering. Nevertheless the experimental results on ^{12}C and ^{208}Pb[3] and on ^4He[4] have been compared with the prediction of calculations within a Δ-hole approach, but the theory was not able to reproduce the experimental data as shown in figs 1, 2, 3 and 4. In the case of ^{12}C and ^{208}Pb since the 10% energy resolution was not sufficient to distinguish elastic from inelastic scattering, some attempts[3,5] have been performed to include the contribution coming from the excitation of the nucleus using various nuclear models. Even if in this case the discrepancy reduces, still the theory is far away from reproducing the data.

It must be noted that these experimental data are certainly affected by a large contribution of π^o-production background.

Photon scattering experiments from proton and from deuteron are of fundamental importance in order to investigate and clarify this process in more complex nuclei.

From the experimental point of view photoscattering from the proton proves to be the most favourable because the recoil proton can be easily observed as well as the scattered photon.

From the theoretical point of view the treatment is much more direct and clean since no Δ-propagation through the nucleus or Fermi motion, Pauli blocking and other effects complicate the calculations.

Several experiments using a proton target have been performed more than twenty years ago and the most recent experiment in the Δ-resonance region was carried out in 1972 by H.Genzel et al[6] at the Bonn 500 MeV Synchrotron. In table 1 from ref.7 is given the number of differential cross section data available in the literature in this energy region.

TABLE 1

$\langle k \rangle$ GeV \ $\langle \theta^*_\pi \rangle$	0°	10°	20°	30°	40°	50°	60°	70°	80°	90°	100°	110°	120°	130°	140°	150°	160°	170°	180°
0.140															1				
0.160															1				
0.180															1				
0.200										1				1	2				
0.220								2		2		1		1	1	1			
0.240							1	2		5		3		4		2			
0.260								1		2					1				
0.280								1		6		1		1					
0.300										1			1		1				
0.320							1	1	2	3		1							
0.340														1					
0.360						1				2									
0.380								1		1		1		1					
0.400						1				1									
0.420								1		3		1		1					
0.440										1									
0.460										1									
0.480									1										
0.500																			

All these experiments used continuous bremsstrahlung photon beams. The experiment of Genzel et al. was first published in 1972 but the results have been reanalyzed and republished in 1976 and the final data appear to be larger than the preliminary ones by about 15% on average. The

recoil proton was measured using a range telescope with a 20 MeV resolution while the scattered photon was detected with a mere 30÷40% resolution. Even if the main contribution of π^o production background was rejected by a proper choice of the endpoint energy of the gamma ray beam and by moving the photon detector to an angle at which it could not be hit by scattered photons, the results are still affected by a small contamination of background and by the uncertainty of the knowledge of the photon intensity.

It is well known that elastic photon-scattering cross section at 0^o is related to the total photoabsorption cross section through the optical theorem and the dispersion relations. The elastic scattering cross section can be written as the square of the modulus of the complex scattering amplitude:

$$\frac{d\sigma}{d\Omega}(E,0^o) = \left| R(E,0^o) \right|^2 = \left| Re\,(R(E,0^o)) + Im\,(R(E,0^o)) \right|^2 \qquad [1]$$

Since the total photoabsorption cross section is given by the optical theorem:

$$\sigma_{\gamma,abs.}(E) = \frac{4\pi\hbar c}{E} Im\,(R(E,0^o)) \qquad [2]$$

one gets

$$Im\,(R(E,0^o)) = \frac{E}{4\pi\hbar c}\ \sigma_{\gamma,\,abs.} \qquad [3]$$

As a consequence of the causality requirements[8] the real and the imaginary part of the scattering amplitude are connected by relations known as dispersion relations:

$$Re\,(R(E,0^o)) = \frac{2}{\pi} P \int \frac{E\ Im\,(R(E',0^o))}{E'^2 - E^2}\ dE' \qquad [4]$$

and

$$Im\,(R(E,0^o)) = \frac{2}{\pi} P \int \frac{E'\ Re\,(R(E',0^o))}{E^2 - E'^2}\ dE' \qquad [5]$$

where P stands for the Cauchy principal value. Under convergency condition for the integral (i.e. the total cross section either approaches a constant at high energy or increases with energy not more rapidly than E^2), using Eq.3, the Eq.4 becomes:

$$Re\,(R(E,0^o)) = Re\,(R(0,0^o)) + \frac{E^2}{2\pi^2\hbar c} P \int \frac{\sigma_{\gamma,abs}(E')}{E'^2 - E^2}\ dE' \qquad [6]$$

The differential cross section at an angle ϑ depends on the multipolarity composition of the transition. If one writes

$$R(E,0) = \sum_{\lambda,L} R_{\lambda,L}(E,0) \qquad [7]$$

where λ marks the electromagnetic nature (λ =E,M) and L is the multipolarity (L=1,2,3...), the angular distribution is given by

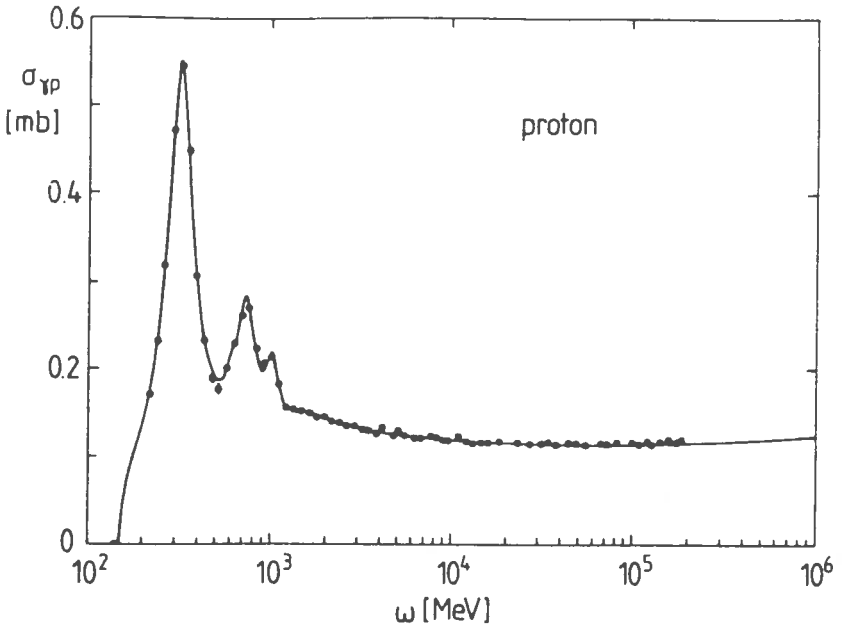

Fig.5 Total photon-proton cross section. The curve is a fit to the data. From ref.9

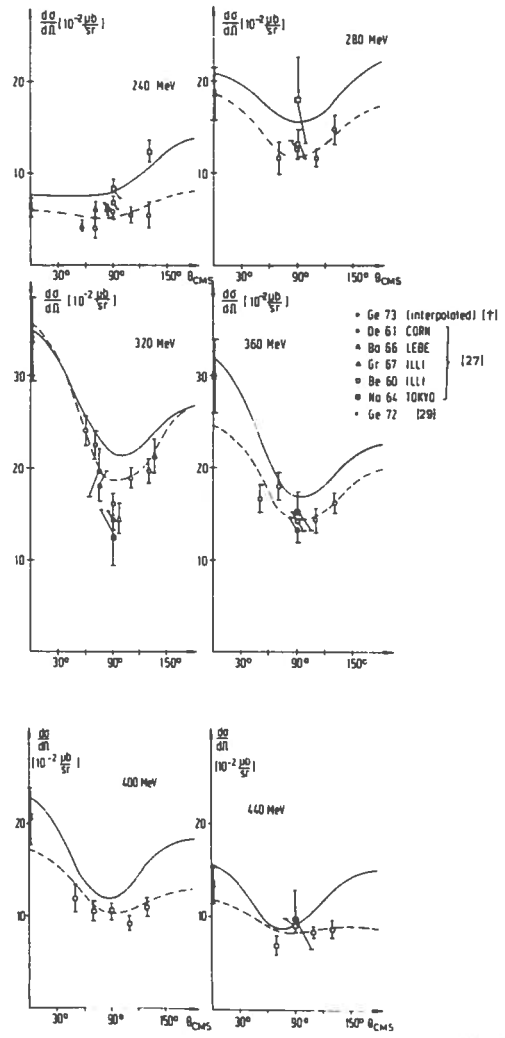

Fig.6 Differential cross section for the photon scattering from proton. Comparison between the experimental data at several photon energies between 240 and 440 MeV and the calculations of ref.10b

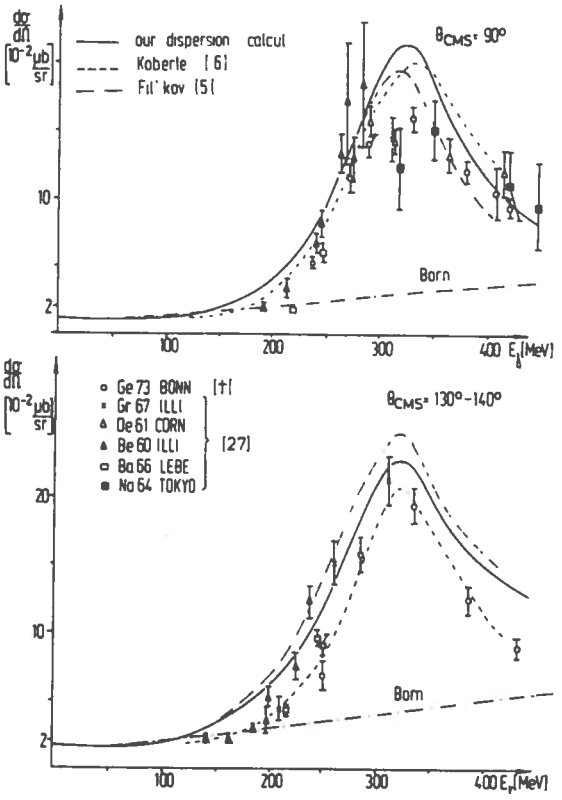

Fig.7 Energy dependence of the cross section for the photon scattering from the proton in the Δ-region. Comparison between the experimental data at $\vartheta^{cms} = 90^o$ and $\vartheta^{cms} = 135^o \pm 5^o$ and the calculations of ref.10b

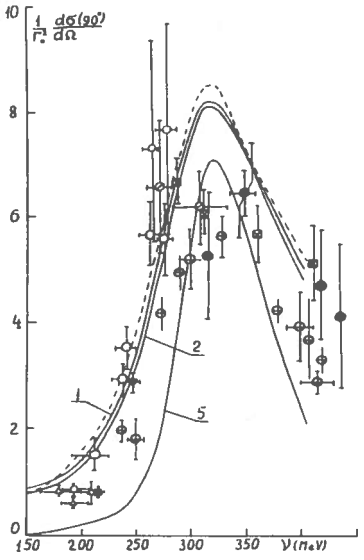

Fig.8 Energy dependence of the cross section for the photon scattering from the proton in the Δ-region. Comparison between the experimental data at $\vartheta^{cms} = 90^{o}$ and the calculations of ref.10c

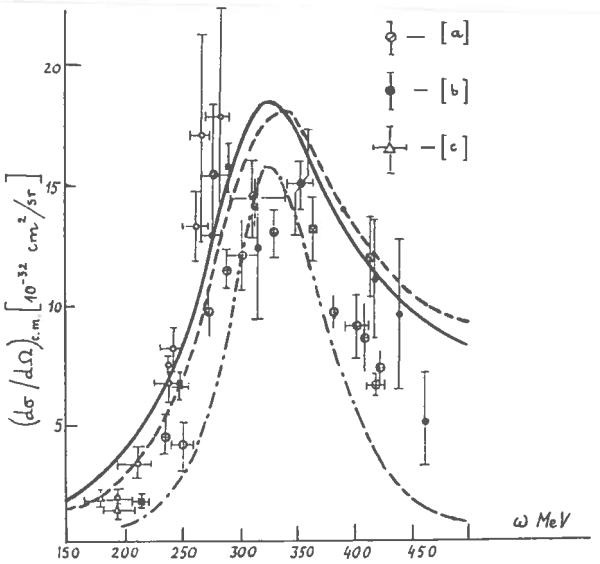

Fig.9 Energy dependence of the cross section for the photon scattering from the proton in the Δ-region.Comparison between the experimental data at $\vartheta^{cms} = 90^{o}$ and the calculations of ref.10

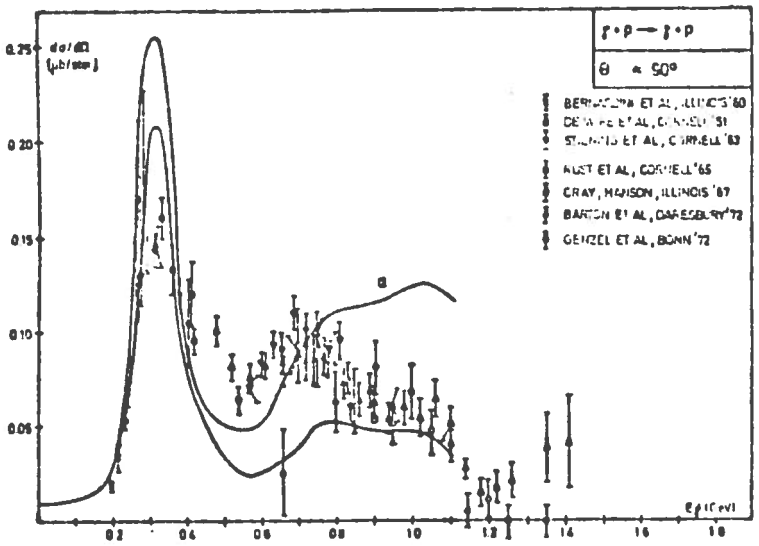

Fig.10 Energy dependence of the cross section for the photon scattering from the proton in the Δ-region. Comparison between the experimental data at $\vartheta^{cms} = 90^{o}$ and the calculations of ref.10e

$$\frac{d\sigma(E,\vartheta)}{d\Omega} = \left| \sum_{\lambda,L} R_{\lambda,L}(E,0^\circ)\, g_{\lambda,L}(\vartheta) \right|^2 \qquad [8]$$

where $g_{\lambda,L}(\vartheta)$ are the angular distribution factors, normalized to be 1 at 0°, which depend not only on the nature and multipolarity of the transition, but also on the spin of the nucleus involved.

The total photoabsorption cross section for the proton has been extensively measured up to energies of the order of 10^6 MeV as shown in fig.5 from ref.9. The multipole decomposition can be deduced from photoproduction experimental results.

Several attempts[10] have been made by different authors to relate the available data on photon-scattering by the proton in the Δ-region to the corresponding photon absorption cross section, through the optical theorem and the dispersion relations. In figs.6 and 7 the experimental results are compared with the theoretical calculations of ref.10b.

The figures show that:

i - The experimental data present a large discrepancy between each other and the results of different experiments at the same incoming photon energy and scattering angle differ for factors even larger than two.

ii - The collection of all data relative to $\vartheta_{cm} = 90^\circ$ shows a Δ-resonance much less prominent than the one measured in the pion photoproduction cross section.

iii - The theory is far away from describing the experimental data.

More advanced theoretical treatments[10 c,d,e], which include the contribution of π^o and η-meson poles, have also not produced agreement with experimental data as shown in figs.8, 9 and 10.

One can conclude that all the attempts to reproduce the photon scattering experimental results using the corresponding photon absorption cross section data have been unsuccessful so far, even if more and more improvements have been done in the treatment of the effects coming from nucleonic mesonic and isobar degrees of freedom.

In order to answer unambiguously the question whether the discrepancy is due to the experimental uncertainty coming from the use of bremsstrahlung beams or to the approximation in the theoretical evaluation and to the effect of subnuclear (quark-gluon) degrees of freedom, a new experiment has been planned which will be presented in the following sections.

2. KINEMATIC CALCULATIONS

When a photon hits a proton target the possible nuclear reactions involved are:

a) $\gamma + p \rightarrow \gamma + p$

b) $\gamma + p \rightarrow \pi^o + p$
$\qquad\qquad\quad \hookrightarrow 2\gamma$

c) $\gamma + p \rightarrow \pi^+ + n$

Both the first and the second reaction give a photon and a proton in the final state and can have similar kinematic conditions.

In the reaction a) the energy $E_{\gamma'}$ of the scattered photon and the energy E_p and the angle ϑ_p of the recoil proton are related to the energy of the incoming photon E_γ by the following formulae:

$$E_{\gamma'} = \frac{m_p c^2 E_\gamma}{E_\gamma + m_p c^2 - E_\gamma \cos\vartheta_{\gamma'}} \qquad [9]$$

$$E_p = E_\gamma - E_{\gamma'} \qquad [10]$$

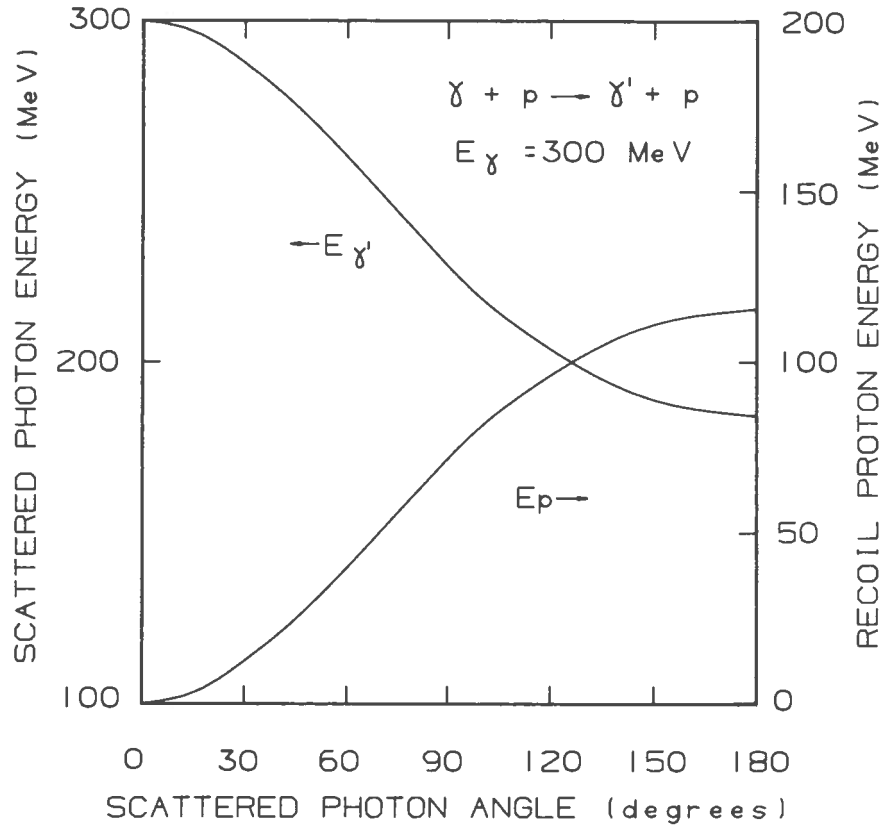

Fig.11 Scattered photon and recoil proton energies as a function of the scattering angle of the photon for the incoming photon energy E_γ = 300 MeV

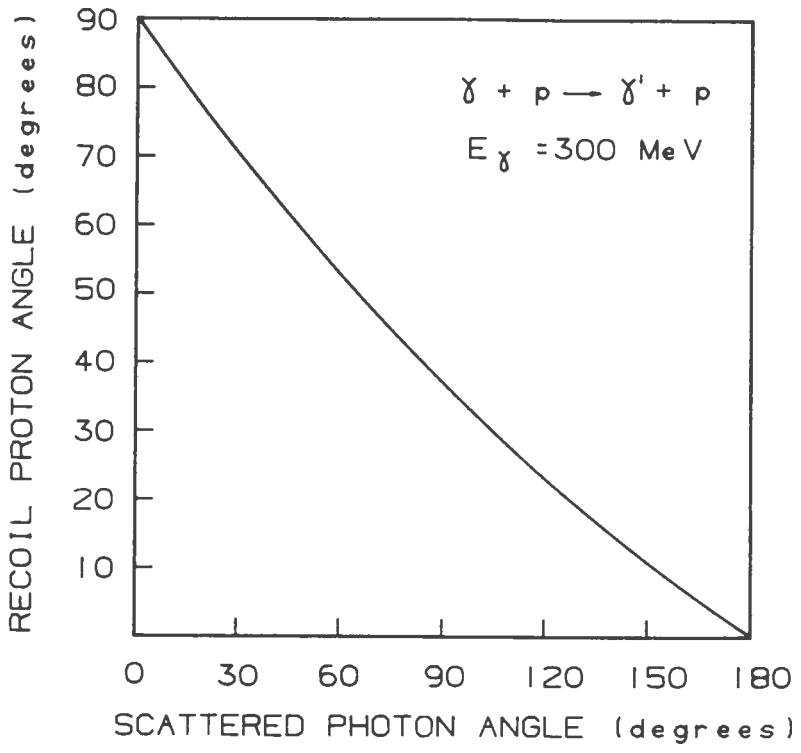

Fig.12 Recoil proton angle as a function of the scattering angle of the photon for the incoming photon energy E_γ = 300 MeV

$$\vartheta_p = \text{acos} \frac{E_\gamma - E_{\gamma'} \cos \vartheta_{\gamma'}}{\sqrt{E_p (E_p\ 2 m_p c^2)}} \quad [11]$$

where $\vartheta_{\gamma'}$ is the angle of the scattered photon.

In fig.11 are shown the dependence of the scattered photon and the recoil proton energy on the photon scattering angle for a fixed incoming photon energy E_γ = 300 MeV. Moreover in fig.12 is reported the dependence of the recoil proton angle on the photon scattering angle for the same incoming photon energy.

It appears from the figures that the proton energy changes very rapidly with the angle, mainly in the region of photon scattering angle between 30^o and 120^o, while the angle of recoil proton varies continuously but only between 0^o and 90^o.

In the reaction b) the energy of recoil proton and the energy and angle of the photoproduced π^o are related to the energy of the incoming photon by the following formulae:

$$E_p = \frac{A(E_\gamma + m_p c^2) + E_\gamma \cos \vartheta_p \sqrt{A^2 - 4m_p^2 c^4 [(E_\gamma + m_p c^2)^2 - E_\gamma^2 \cos^2 \vartheta_p]}}{2 [(E_\gamma + m_p c^2)^2 - E_\gamma^2 \cos^2 \vartheta_p} \quad [12]$$

$$\text{with } A = 2 m_p c^2 (m_p c^2 + E_\gamma) - m^2_{\pi o} c^4 \quad [13]$$

$$E_{\pi o} = E_\gamma - E_p - M_{\pi o} c^2 \quad [14]$$

$$\vartheta_{\pi o} = \text{acos} \frac{E_\gamma - \sqrt{E_p (E_p + 2 m_p c^2)} \cos \vartheta_p}{\sqrt{E_{\pi o} (E_{\pi o} + 2 m_{\pi o} c^2)}} \quad [15]$$

where ϑ_p is the angle of the recoil proton.

In fig.13 are reported the energies of protons emitted in the reactions a) and b) as a function of the emission angle for the incoming photon energy E_γ = 300 MeV. The figure shows that the two reactions give very similar energy-angle dependence.

The energy of photons from the decay of π^o is related to the energy E_{π^o} of π^o and to the emission angle $\vartheta_{\gamma \pi^o}$ of the photon with respect to the π^o direction by the following formulae:

$$E_{\gamma'} = \frac{m^2_{\pi o} c^4}{2} \frac{1}{(E_{\pi o} + m_{\pi o} c^2) - \sqrt{E_{\pi o} (E_{\pi o} + 2 m_{\pi o} c^2) \cos \vartheta_{\gamma'}}} \quad [16]$$

$$E_{\gamma''} = E_{\pi o} + m_{\pi o} c^2 - E_{\gamma'} \quad [17]$$

$$\vartheta_{\gamma''} = \text{acos} \frac{\sqrt{E_{\pi o} (E_{\pi o} + 2 m_{\pi o} c^2)} - E_{\gamma'} \cos \vartheta_{\gamma'}}{E_{\gamma''}} \quad [18]$$

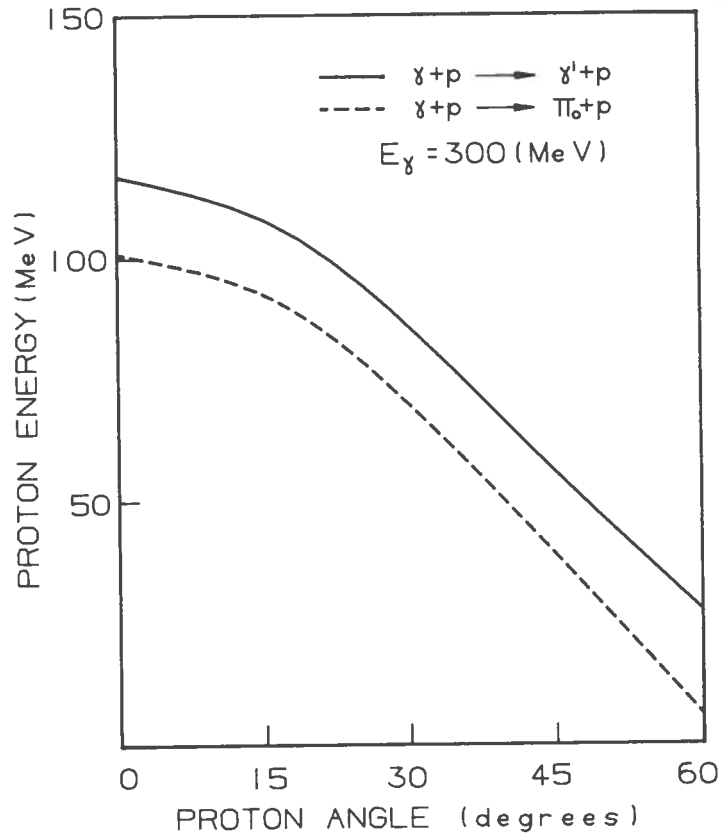

Fig.13 Energies of the recoil protons in the photon-scattering and π^0-production reactions as a function of the emitted angle for the incoming photon energy E_γ = 300 MeV

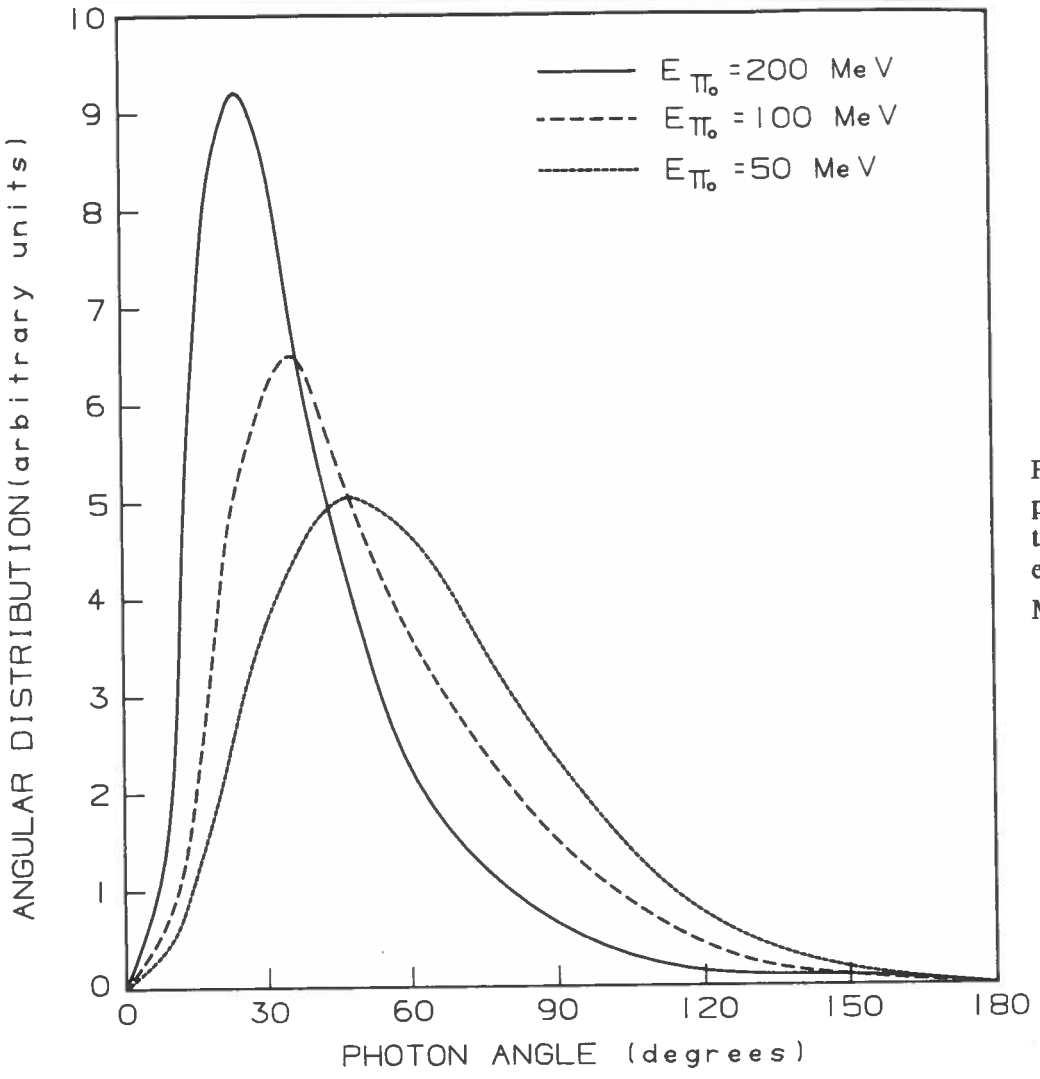

Fig.14 Angular distribution of the photon from π^0-decay relative to the π^0 direction and for the π^0 energies E_{π^0} = 50, 100 and 200 MeV

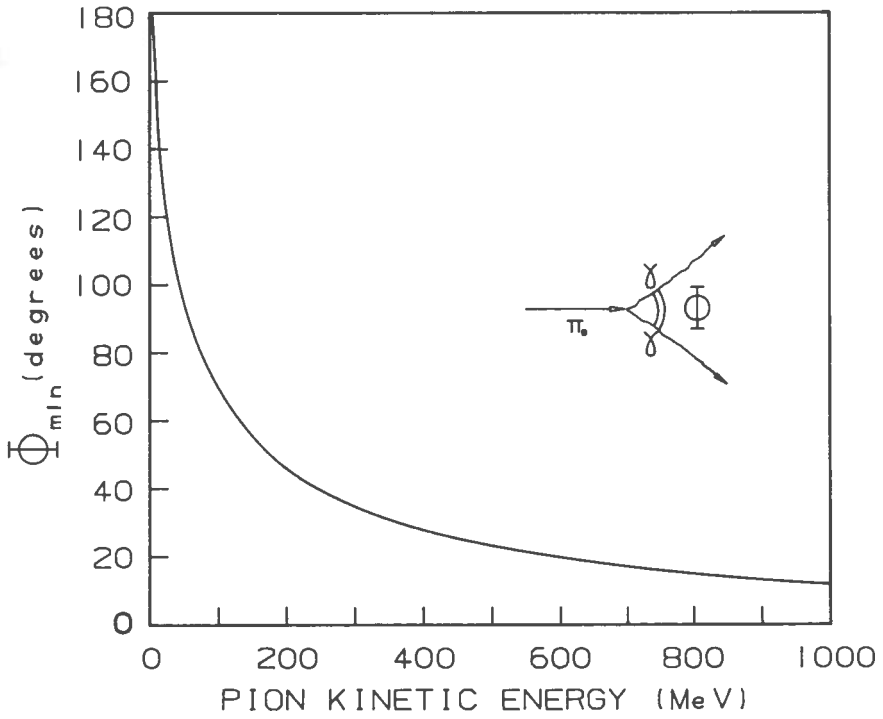

Fig.15 Minimum angle between the two photons from the π^0-decay as a function of π^0 energy.

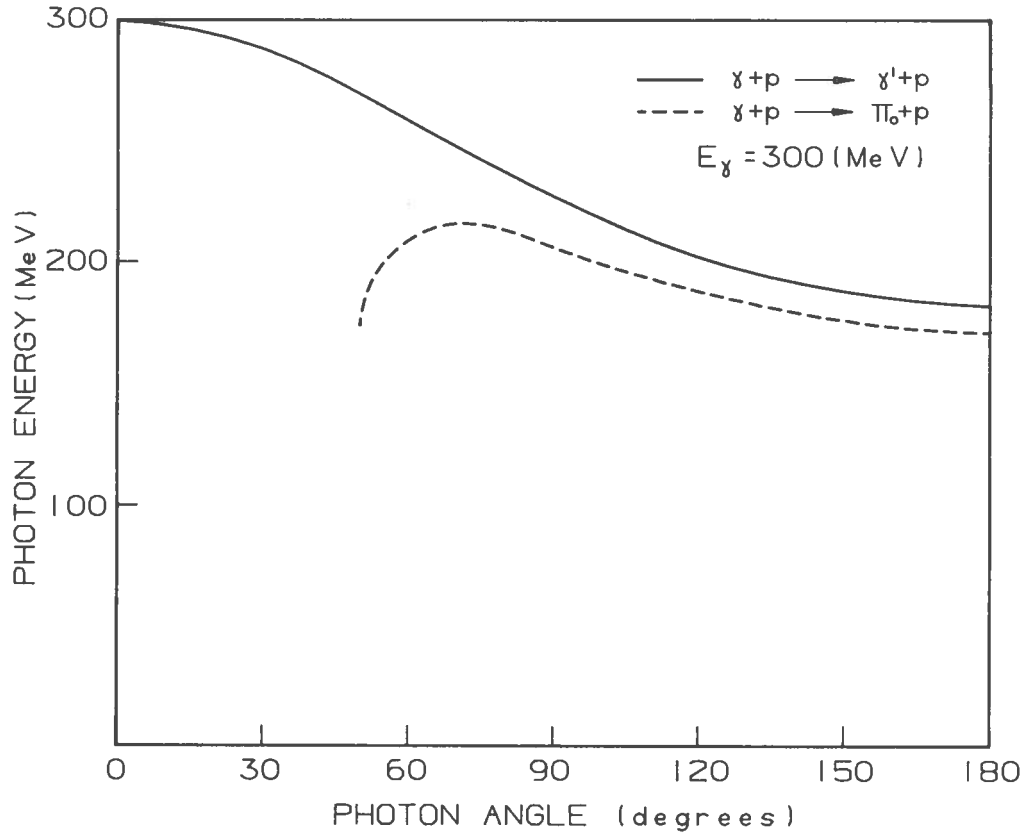

Fig.16 Energies of the photons in the photon-scattering and the π^0-production reactions as a function of the emitted angle for the incoming photon energy E_γ = 300 MeV

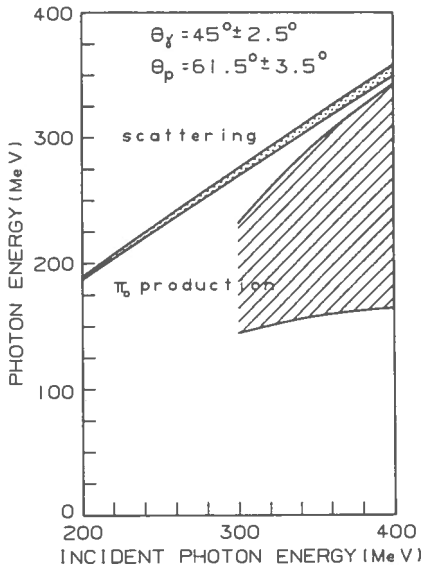

Fig.17 Energy distribution of the photons from the photon-scattering and the π^0-production reactions as a function of the incident photon energy for the emitted photon angle $\vartheta_\gamma = 45^0 \pm 2.5^0$ and the recoil proton angle $\vartheta_p = 61.5^0 \pm 3.5^0$

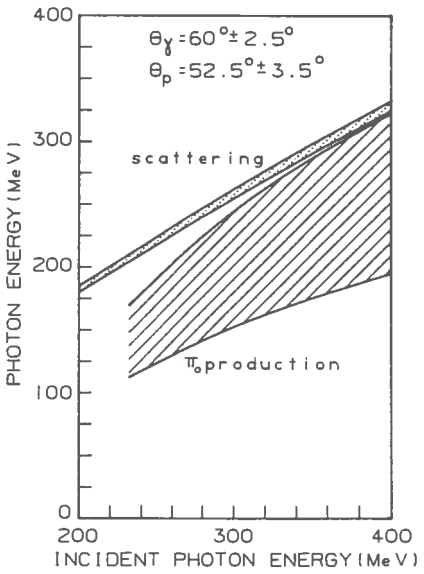

Fig.18 The same as fig.17 for the emitted photon angle $\vartheta_\gamma = 60^0 \pm 2.5^0$ and the recoil proton angle $\vartheta_p = 52.5^0 \pm 3.5^0$

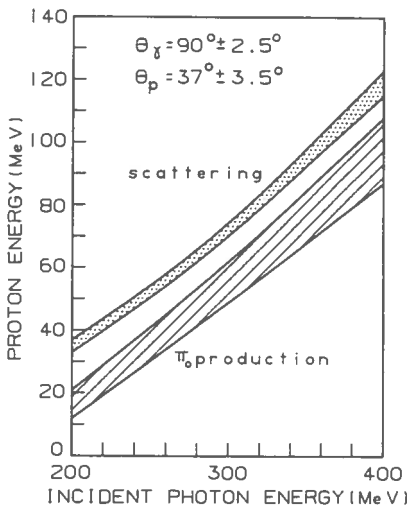

Fig.19 The same as fig.17 for the emitted photon angle $\vartheta_\gamma = 90^0 \pm 2.5^0$ and the recoil proton angle $\vartheta_p = 37^0 \pm 3.5^0$

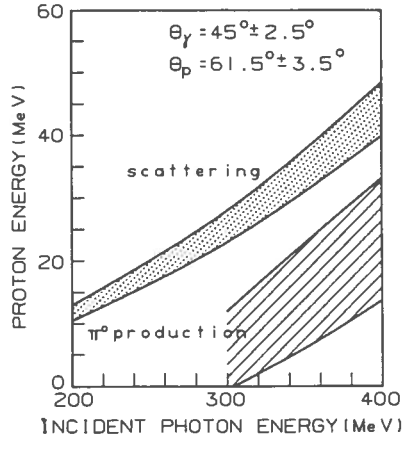

Fig.20 Energy distribution of the protons from the photon-scattering and the π^0-production reactions as a function of the incident photon energy for the emitted photon angle $\vartheta_\gamma = 45^0 \pm 2.5^0$ and the recoil proton angle $\vartheta_p = 61.5^0 \pm 3.5^0$

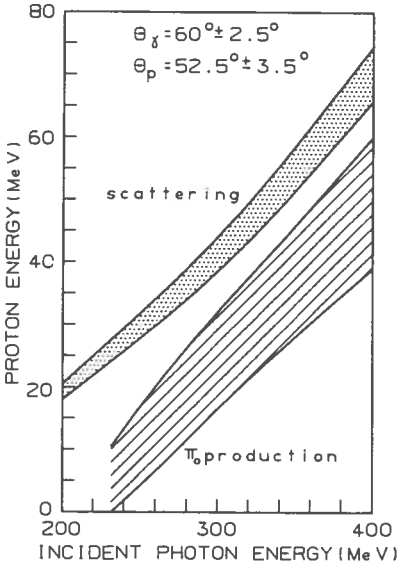

Fig.21 The same as fig.20 for the emitted photon angle $\vartheta_\gamma = 60^0 \pm 2.5^0$ and the recoil proton angle $\vartheta_p = 52.5^0 \pm 3.5^0$

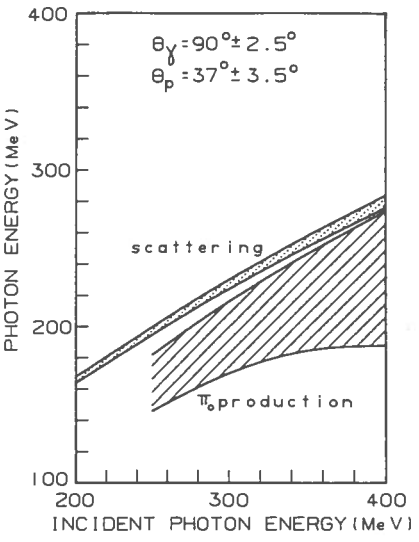

Fig.22 The same as fig.20 for the emitted photon angle $\vartheta_\gamma = 90^0 \pm 2.5^0$ and the recoil proton angle $\vartheta_p = 37^0 \pm 3.5^0$

Even if in the centre of mass system the photons are emitted isotropically, in the laboratory system this is no more true and the angular distribution of photons depends on the π^o energy as shown in fig.14. The probability of photon emission is always zero at $\vartheta_{\gamma\pi^o} = 0^o$ and has a maximum at $\vartheta_{\gamma\pi^o} = \Phi_{min}/2$. Φ_{min} is the minimum angle between the two photons in the laboratory system, which is given by

$$\Phi_{min} = 2\,\mathrm{atg}\,\frac{m_{\pi o}c^2}{\sqrt{E_{\pi o}(E_{\pi o} + 2\,m_{\pi o}c^2)}} \qquad [19]$$

The value of Φ_{min} as a function of π^o energy is presented in fig.15.

It is clear that it does not exist a unique relationship between the energy of a photon from π^o decay and its angle of emission $\vartheta_\gamma^{(\pi o)}$ with respect to the incoming photon direction. To have a unique relationship it is necessary to give more kinematic conditions, as for example by fixing the π^o direction or the proton direction. In the latter case one can choose for each $\vartheta_\gamma^{(\pi o)}$ the proton emission angle $\vartheta_p^{(\pi o)}$ given by the kinematic relationship [11] relative to photon scattering process and already shown in fig.12.

The resulting dependence of the photon energy on its emission angle is then represented in fig.16 relative to the incoming photon energy $E_\gamma = 300$ MeV. In the figure is also reported the dependence of the scattered photon energy from the process a) on the scattering angle for comparison. It appears that the two reactions a) and b) give very similar energy-angle dependence also for photons.

Since in a real experiment the dimensions of the detector give a finite angular resolution, in fig.17,18,19,20,21 and 22 are shown the energy distributions of photons and protons from process a) and b) relative to three different photon emission angles: $\vartheta_\gamma + \Delta\vartheta_\gamma = 45^o \pm 2.5^o$, $60^o \pm 2.5^o$ and $90^o \pm 2.5^o$ respectively. In this evaluation the angle and the collimation for the protons have been chosen in order to collect all the protons from scattering process.

The relationship between $\vartheta_p^{(scatt)}$ and $\vartheta_\gamma^{(scatt)}$ depends on the incoming photon energy as shown in fig.23. Since this dependence changes very slowly it is sufficient to fix the same proton-detector direction for the whole incoming photon energy range between 200 and 400 MeV and a collimator angle a little larger than the photon collimation one, instead of changing the detector proton direction as a function of the incoming photon energy.

Figures 17÷22 show that a larger $\Delta\vartheta_\gamma$ collimation would produce overlap between the two energy distributions particularly for the photons, and would not allow to separate further the contribution of the two processes.

The relationship between the scattered photon angle in the laboratory system ϑ_γ^{lab} and in the centre of mass system, ϑ^{cms} can be evaluated starting from:

$$\vartheta^{cms} = \mathrm{acos}\,\frac{(1-\rho^2)\cos\vartheta_\gamma^{lab} - \rho\sin^2\vartheta_\gamma^{lab}}{1-\rho^2\cos^2\vartheta_\gamma^{lab}} \qquad [20]$$

$$\text{with} \quad \rho = \frac{E_\gamma}{E_\gamma + m_p c^2} \qquad [21]$$

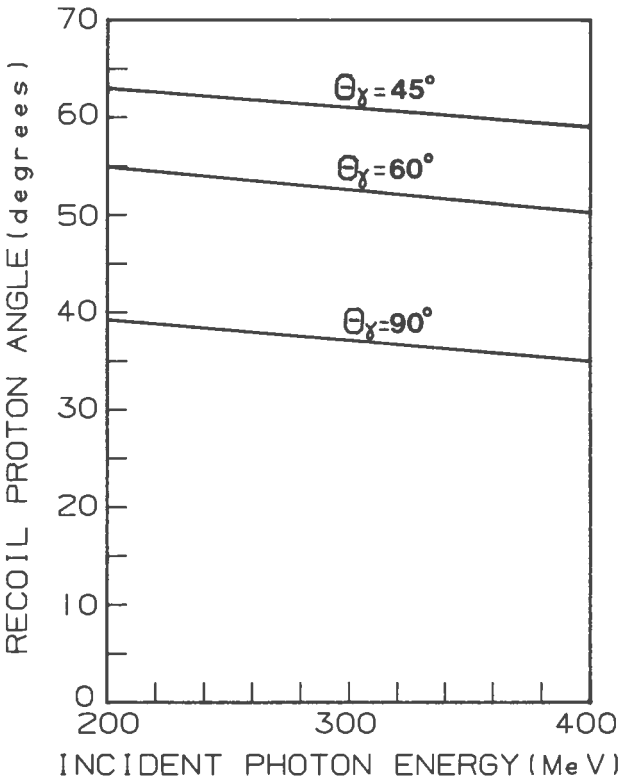

Fig.23 Recoil proton angle as a function of the incoming photon energy for the scattering angle of the photon $\vartheta_\gamma^{scatt} = 45^o$, 60^o and 90^o

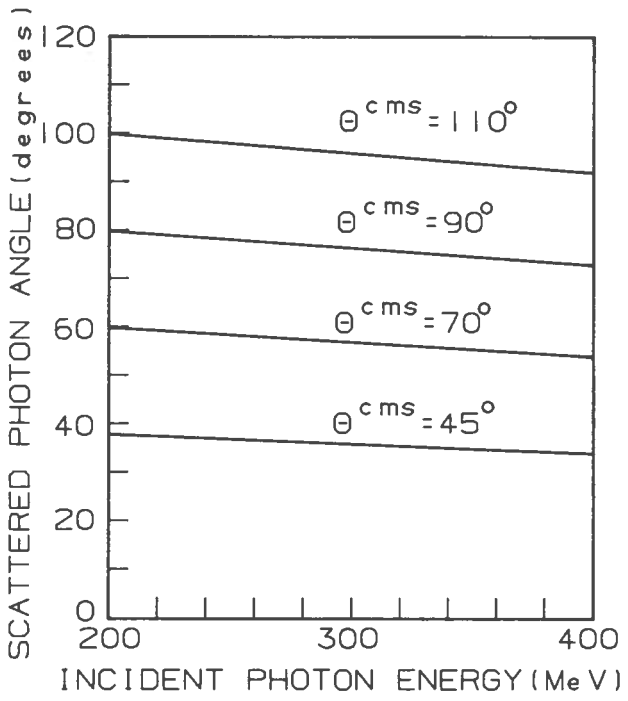

Fig.24 Scattering angle of the photon in the laboratory system as a function of the incident photon energy for the scattering angle in the centre of mass system $\vartheta^{cms} = 45^o$, 70^o, 90^o and 110^o

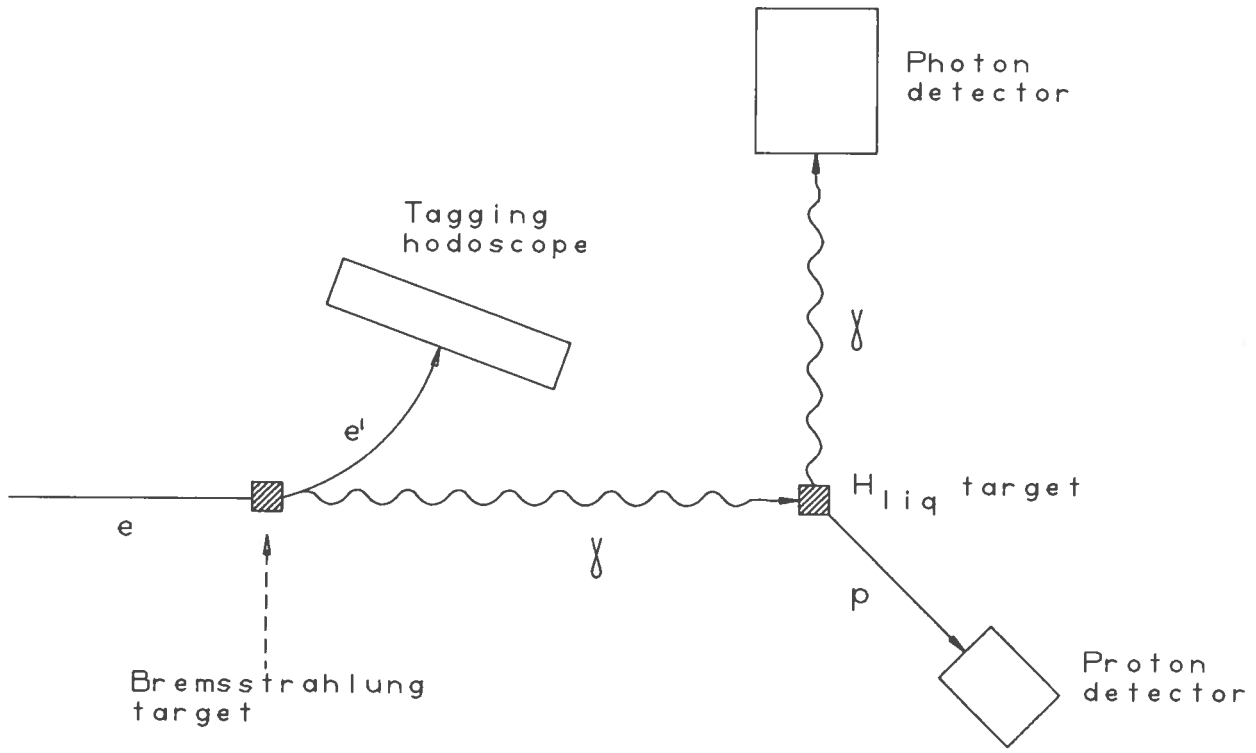

Fig.25 Layout of the experimental arrangement. The scattered photon and the recoil proton are detected in coincidence with the electron in the tagging hodoscope

It has been evaluated for four different ϑ^{cms} angles and between E_γ = 200 MeV and 400 MeV and the results are presented in fig.24. It shows that the relationship is very slowly dependent on the incoming photon energy.

3. EXPERIMENTAL ARRANGEMENT

The experiment will be performed using monochromatic tagged photons. Moreover the included scattered photon and the recoil proton will be detected at the same time. This means that it will be a triple coincidence arrangement, as shown in fig.25. The energy range of the tagged photons will be between 200 and 400 MeV.

The possible reaction channels, when a photon in this energy range impinges on an Hydrogen target are the following.

i - nuclear processes:

a) $\gamma + p \rightarrow \gamma + p$

b) $\gamma + p \rightarrow \pi^o + p$
$\quad \hookrightarrow 2\gamma \; (T_{\frac{1}{2}} \cong 10^{-16}\,\text{sec})$

c) $\gamma + p \rightarrow \pi^+ + n$

ii - atomic processes:

d) $\gamma + e \rightarrow \gamma' + e'$
$\quad \hookrightarrow$ bremsstrahlung γ

$\gamma\,(+N) \rightarrow e^+ + e^-\,(+N)$
$\quad \hookrightarrow \; \hookrightarrow$ bremsstrahlung γ

With the exception of c) all these processes produce photons which can give a background in the photon detector.

The advantages of a triple coincidence arrangement are

i - The complete rejection of the background coming from atomic processes, cosmic rays, reactions in the H_{liq} target walls, etc.

ii - The good discrimination between the two processes
$\gamma + p \rightarrow \gamma + p$ and $\gamma + p \rightarrow \pi^o + p$

iii - The reduction of accidental coincidences without reduction of true coincidences.

The advantage of using tagged photons are:

iv - The good precision for the monitoring of the incoming photon intensity

v - The simultaneous measurement in the whole energy region $E_\gamma = 200 \div 400$ MeV

Two angles in the centre of mass system will be selected: $\vartheta^{cms} = 90^o$ and $\vartheta^{cms} = 70^o$.

The corresponding ϑ_γ^{lab} and ϑ_p^{lab} are presented in table 2

TABLE 2

ϑ^{cms} (degrees)	ϑ_γ^{lab} (degrees)	ϑ_p^{lab} (degrees)
90	76 ± 4	44 ± 2
70	57 ± 3.5	54.5 ± 2

In the experimental arrangement the detectors will have an angular acceptance smaller than that given in table 2. This is due to the requirement of a good separation between the products of the two reactions: photon scattering and π^o production. In any case, since the differential cross section depends very smoothly on the angle, this choice will not affect the measurement.

To evaluate the expected recoil proton and scattered photon energy distribution in the experimental condition, a Monte-Carlo simulation has been performed. Input data of the program are the differential cross section for the reaction $\gamma + p \rightarrow \pi^o + p$ taken from ref.7 and an approximate value of the cross section for the reaction $\gamma + p \rightarrow \gamma + p$. The program evaluated the kinematics of the two processes and of the $\pi^o \rightarrow 2\gamma$ process and the energy loss of protons in the Hydrogen target. Moreover it evaluates the effects of the extended target geometry, of the photon beam size and spatial intensity distribution in the beam, of the energy indetermination of the incident photons and of the dimensions of photon and proton detectors.

The results of the Monte-Carlo simulation are presented in figs. $26 \div 33$ for two incoming photon energies and for the two selected angles. These results are relative to a cylindrical liquid Hydrogen target, with 2 cm diameter and 6 cm length, and to a photon detector angular acceptance $\pm 2.5^o$ both in the radial and in the azimuthal planes, placed at 1.8 m distance from the target and to proton detector angular acceptance $\pm 3.5^o$ in the radial plane and $\pm 2.5^o$ in the azimuthal plane, placed at 1 m distance from the target. Moreover the photon beam intensity has a Gaussian distribution with $\sigma = 4$ mm and the energy indetermination is $\Delta E_\gamma / E_\gamma = 3\%$.

Fig.34 shows the proton energy distribution in the whole range of the tagged photons $E\gamma = 200 \div 400$ MeV.

Figs.$26 \div 34$ show that in these experimental conditions there will be a good discrimination between the two reaction products for what concerns the proton spectra for all the photon energies and at both angles. On the contrary the peak of the scattered photon energies and the energy distribution relative to the π^o production overlap mainly for incoming photon energy above 300 MeV.

As a consequence the discrimination between the two processes is possible only by analyzing the proton energy distribution and using a proton detector with a resolution of a few percents, while the photon detector will be needed for defining the kinematics of the event.

Using the Monte-Carlo simulation the effects on the proton spectra due to the dimensions of the H_{liq} target, to the characteristics of the photon beam and to the distance between target and detectors have been evaluated.

The effect of the target length is presented in figs.35 and 36. Fig.35 shows the proton energy distributions for a target length of 6 cm and 10 cm relative to incident photon energy $E_\gamma = 400$ MeV and $\vartheta_\gamma^{lab} = 76^o$. It appears that the increase of the target length does not affect the separation between the two processes products even at $E_\gamma = 400$ MeV, which represents the most critical condition. Obviously the efficiency of the detection apparatus decreases when the target length increases, as shown in fig.36. As a consequence the expected counting rate of the experiment is not proportional to the target length.

The diameter of the Hydrogen target must be chosen according to the size of the photon beam. Therefore to evaluate the effect of the target diameter different beam dimensions have been

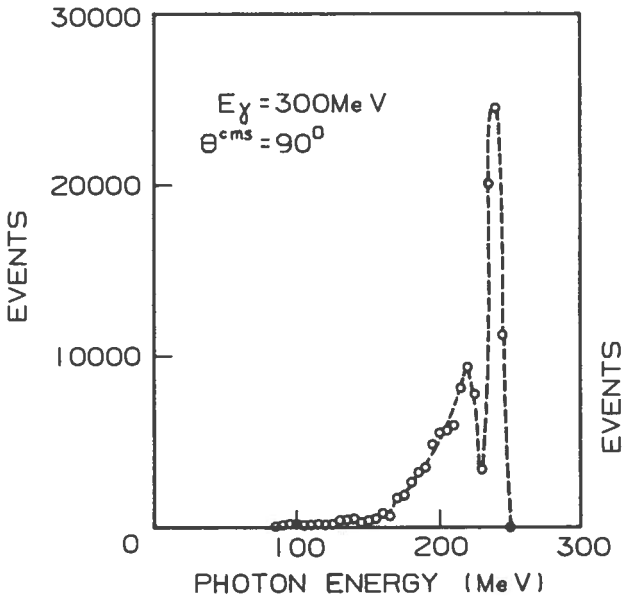

Fig.26 Result of a Monte-Carlo simulation for the photon energy distribution relative to the incoming photon energy $E_\gamma = 300$ MeV and $\vartheta^{cms} = 90^o$

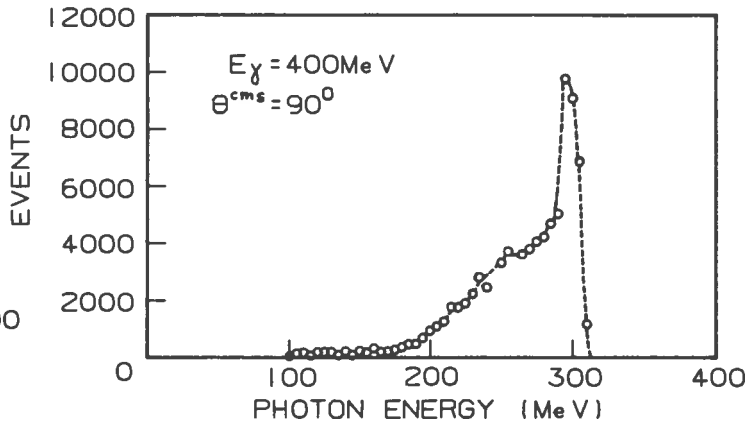

Fig.27 The same as fig.26 relative to the incoming photon energy $E_\gamma = 400$ MeV and $\vartheta^{cms} = 90^o$

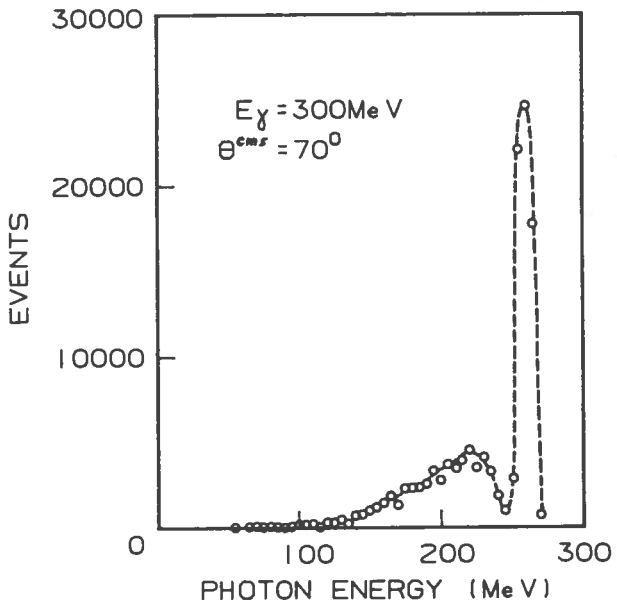

Fig.28 The same as fig.26 relative to the incoming photon energy $E_\gamma = 300$ MeV and $\vartheta^{cms} = 70^o$

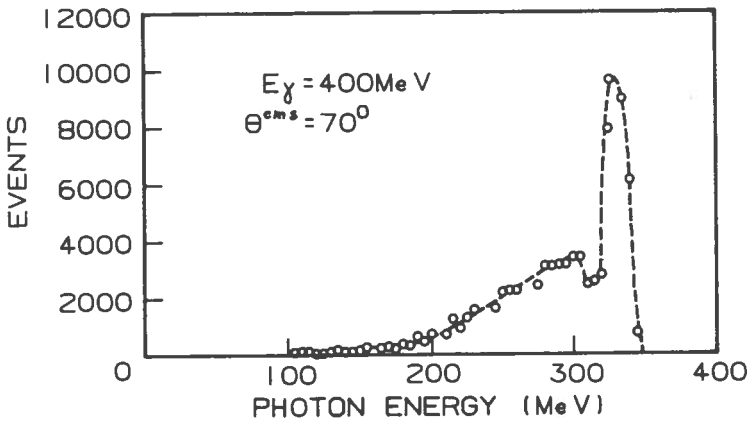

Fig.29 The same as fig.26 relative to the incoming photon energy $E_\gamma = 400$ MeV and $\vartheta^{cms} = 70^o$

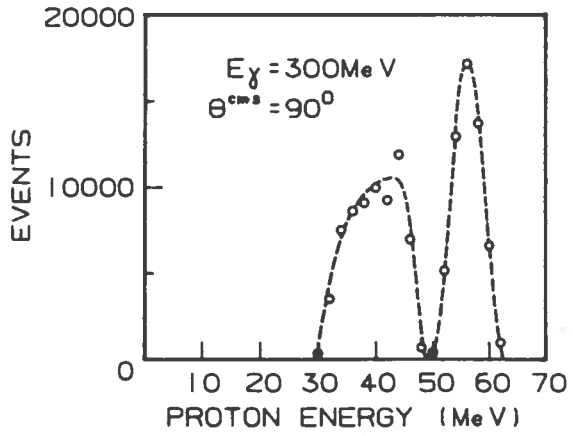

Fig.30 Result of a Monte-Carlo simulation for the proton energy distribution relative to the incoming photon energy $E_\gamma = 300$ MeV and $\vartheta^{cms} = 90^o$

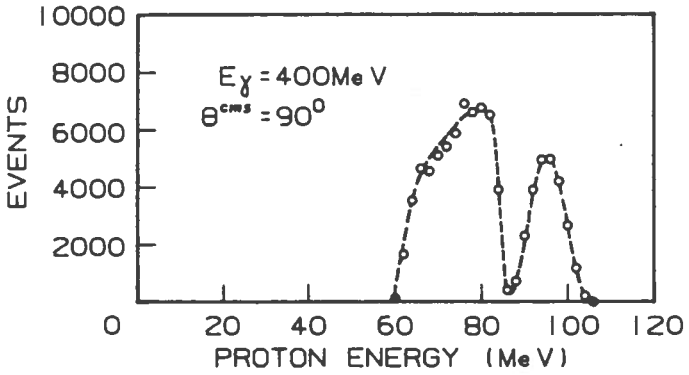

Fig.31 The same as fig.30 relative to the incoming photon energy $E_\gamma = 400$ MeV and $\vartheta^{cms} = 90^o$

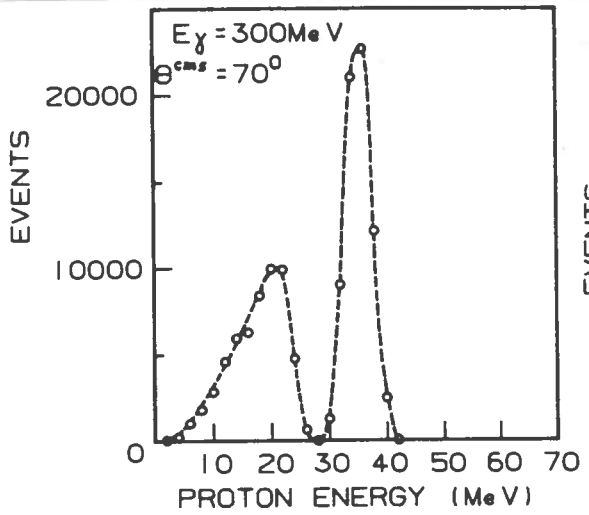

Fig.32 The same as fig.30 relative to the incoming photon energy $E_\gamma = 300$ MeV and $\vartheta^{cms} = 70^o$

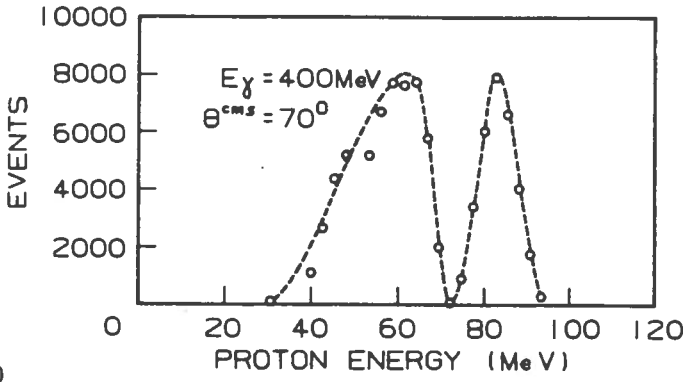

Fig.33 The same as fig.30 relative to the incoming photon energy $E_\gamma = 400$ MeV and $\vartheta^{cms} = 70^o$

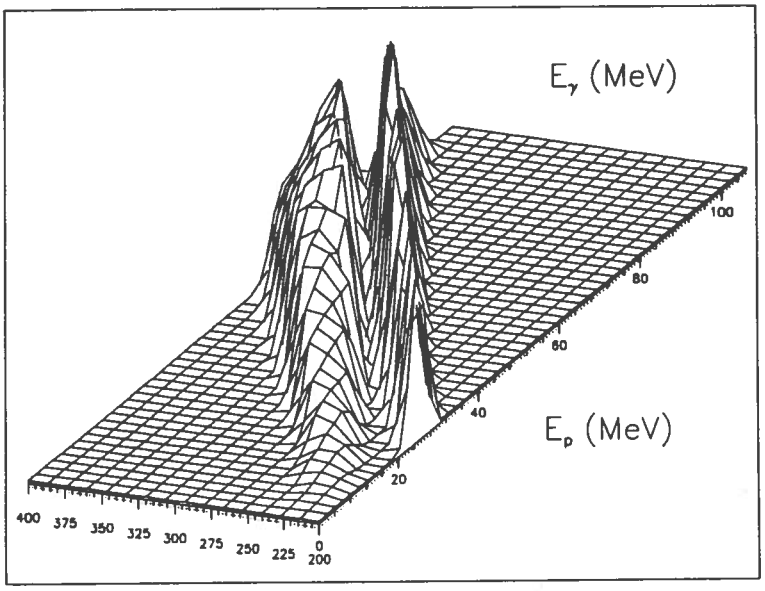

Fig.34 Result of Monte-Carlo simulation for the proton energy distribution in the range of the incoming photon energy $E_\gamma = 200 \div 400$ MeV relative to $\vartheta^{cms} = 90^o$

considered and the target diameter has been changed consequently. Once more the photon beam intensity was assumed to have a Gaussian distribution. Obviously this effect will contribute only to the proton spectrum and will be more important as the energy of the proton decreases.

In table 3 are reported the values of σ for the Gaussian distribution and of the target diameter d, chosen for the calculation.

TABLE 3

σ (mm)	d(cm)
4	1.6
6	2.4
9	4

Fig.37 shows the result for the proton energy distribution relative to incident photon energy $E_\gamma = 250$ MeV and $\vartheta_\gamma^{lab} = 76°$. It appears that the increase of the target diameter and consequently of the energy loss of protons in the target do not affect the separation between the two processes products, even at $E_\gamma = 250$ MeV, which represents the most critical condition.

Finally in fig.38 is shown the effect of varying the distance between target and detectors. In the calculation the solid angle of both photon and proton detectors was not changed. In this case the effect can only be due to the dimensions of the target, since for a pointlike target no contribution must be expected. In the calculations relative to fig.38 only the distance of the photon detector has been changed and decreased from 180 cm to 150 cm. From the figure it appears that there is no difference in the proton energy spectrum, even at $E_\gamma = 400$ MeV, which represents the most critical condition.

It is obvious that in the $\gamma + p \rightarrow \gamma + p$ process the incoming photon, the recoil proton and the scattered photon lie necessarily in a plane, which is defined as "reaction plane". This is not true for the incoming photon, the recoil proton and a photon from the π^o decay in the $\gamma + p \rightarrow \pi^o + p$ process. This means that, if one evaluates the energy distribution of protons and photons when one of the detectors is placed out of the "reaction plane", one expects no contribution from the scattering reaction but some contribution from the other process.

This contribution has been evaluated using the Monte-Carlo simulation and placing the photon detector at different azimuthal φ angle ($\varphi = 0°$ in the "reaction plane"). Some results are presented in the figs.39÷44 for the azimuthal angles $\varphi = 0°$ and $\varphi = 10°$. The figures show the photon and proton spectra at $E_\gamma = 400$ MeV for $\vartheta_\gamma^{lab} = 76°$ and $\vartheta_\gamma^{lab} = 57°$ and the proton spectra at $E_\gamma = 250$ MeV for the same two ϑ_γ^{lab} and for $\varphi_\gamma = 0°$ and $\varphi_\gamma = 10°$. In the figures the spectra relative to $\varphi = 10°$ have been normalized by a factor which depends on φ and ϑ_γ angles.

It appears from the figures that the energy distributions of the recoil proton from the π^o production process are the same when φ changes from $\varphi = 0°$ and $\varphi = 10°$, at least for what concerns the shape. On the contrary the photon energy distribution seems to be very sensitive to the azimuthal angle.

This result should not surprise since, as one has seen in fig. 14 of Section 2, the probability of photon emission for the π^o decay has a maximum value for $\vartheta_{\gamma\pi_o} = \Phi_{min}/2$ and goes to zero at $\vartheta_{\gamma\pi^o} = 0°$. This means that, as long as the azimuthal angle is smaller than $\Phi_{min}/2$, there cannot be

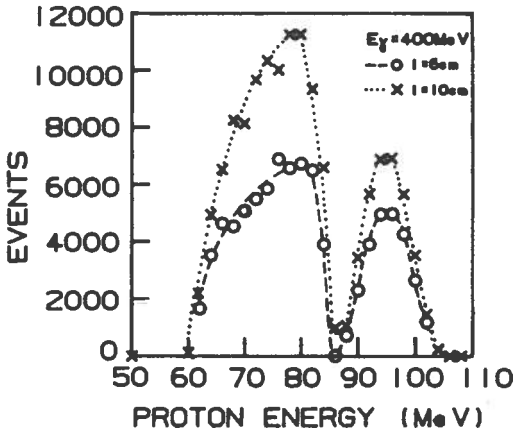

Fig.35 Result of a Monte-Carlo simulation for the proton energy distribution relative to the incident photon energy $E_\gamma = 400$ MeV, $\vartheta^{cms} = 90^o$ and the Hydrogen target length l = 6 and 10 cm

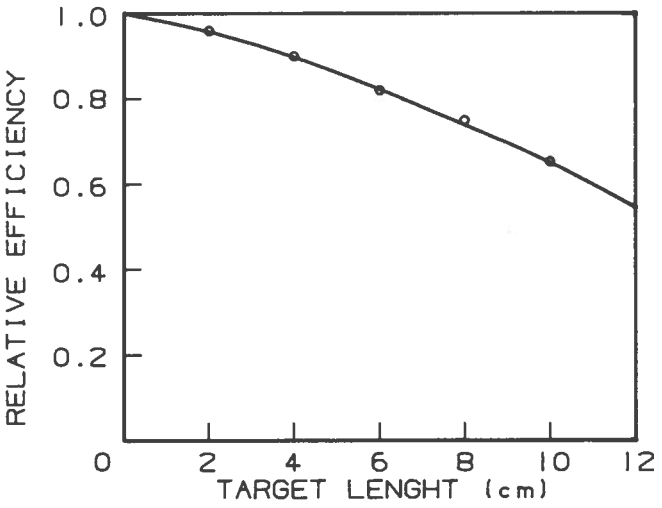

Fig.36 Result of a Monte-Carlo simulation for the relative efficiency of the apparatus as a function of the Hydrogen target length relative to $E_\gamma = 400$ MeV and $\vartheta^{cms} = 90^o$

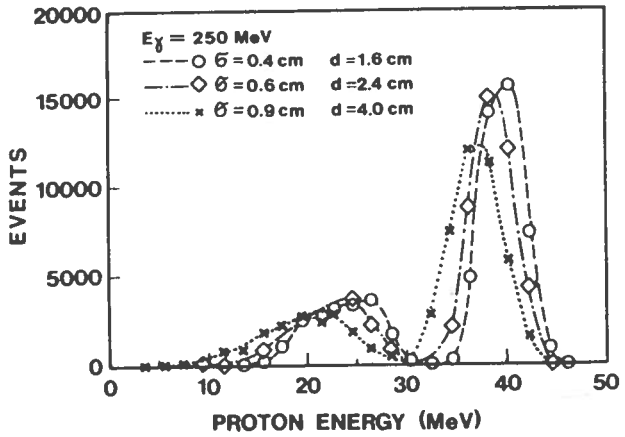

Fig.37 Result of a Monte-Carlo simulation for the proton energy distribution relative to the incident photon energy $E_\gamma = 250$ MeV, $\vartheta^{cms} = 90^o$ and the Hydrogen target diameter d = 1.6, 2.4 and 4 cm

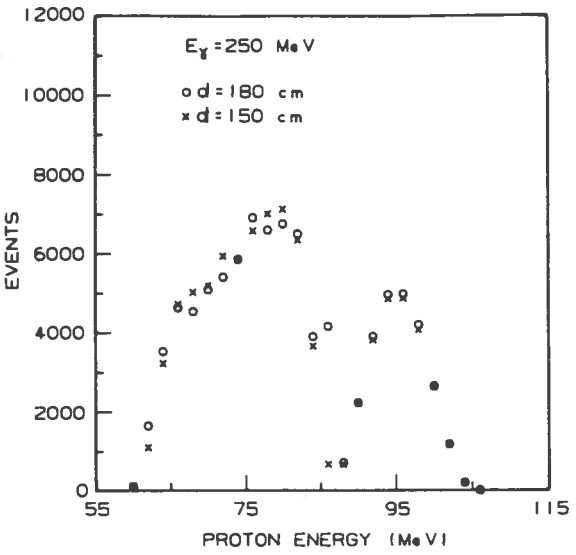

Fig.38 Result of a Monte-Carlo simulation for the proton energy distribution relative to the incident photon energy $E_\gamma = 400$ MeV, $\vartheta^{cms} = 90^o$ and the distance between Hydrogen target and photon detectors d = 150 and 180 cm

a drastic change in the kinematical condition of the detected events concerning the π^o production process, and only the number of events changes. This is shown in fig.45 where the number of events as a function of φ is given for $E_\gamma = 400$ MeV and $\vartheta_\gamma^{lab} = 76^o$, as an example.

The ratio R(0°/ 10°) between the events detectable at $\varphi = 0^o$ and $\varphi = 10^o$ does not depend on the incoming photon energy in the interval E_γ 200 ÷ 400 MeV as shown in fig.46.

The calculation results obtained for the proton spectra in and out of the "reaction plane" are very important. As a consequence it is possible in principle to subtract the background contribution due to the π^o production, even if one does not analyze the proton spectrum, but just using two photon detectors having the same characteristics and placed at the same ϑ but at different φ, that is $\varphi = 0^o$ and $\varphi = 10^o$.

4. APPARATUS DESCRIPTION.

As already written in section 3 the experiment will be performed using tagged photons. The scattered photon and the recoil proton are detected in coincidence with the electron in the tagging hodoscope.

The discrimination between events coming from the elastic scattering process and events due to π^o production is performed using a telescope ΔE, E of plastic scintillator counters to detect protons.

This kind of spectrometer is expected to have a resolution of a few percent at the energies involved in the experiment. The photons are detected by Cerenkov lead-glass counters, since we have already seen in section 3 that a good resolution is not necessary for the photon detector in the arrangement of this experiment.

A plastic scintillator detector, 1 cm thick, is placed in front of the lead-glass counter, in order to reject, by operating in anticoincidence, the charged background. The advantages of this kind of detectors are the high efficiency available, the possibility of easily obtaining a fast coincidence and the relative low cost.

Cost is of some importance, since the whole apparatus consists of many detectors. In fact we have seen in the sections 2 and 3 that, in order to discriminate between the two competitive processes $\gamma + p \rightarrow \gamma + p$ and $\gamma + p \rightarrow \pi^o + p$, the angular acceptance of each detector must be small. We have chosen a solid angle $\Delta\Omega = 7$ msr. Then in order to reduce the effect of the target dimensions on the kinematic definition it is necessary to have a distance between target and detectors of the order of a meter, at least. Therefore the detectors must have a large surface. Moreover in order to obtain a reasonable counting rate, the total solid angle must be of the order of 40 ÷ 50 msr, as we will discuss later.

As a consequence for each scattering angle are employed 6 lead-glasses and 6 scintillator telescopes.

Each lead-glass crystal is a block of 15 x 15 x 30 cm^3. The layout of this detector is shown in fig.47. These Cerenkov lead-glasses were already employed in an experiment of Particle Physics at ISR[12]. In fig.48 is shown the response of this kind of detectors to cosmic-rays and to monochromatic photons, as measured at the Saclay Linac using the photon beam from the annihilation of positron.

Each plastic-scintillators for E_p analysis is a cylinder of diameter 15 cm and height 14 or 8 cm. The layout of this detector is presented in fig.49. The resolution of this kind of detector is ~ 2.5% at $E_p = 100$ MeV. It has been measured between 20 and 30 MeV at the Legnaro Laboratory Tandem using the protons scattered at 15° by ^{12}C. In fig.50 the response to proton for $E_p = 25$ and 30 MeV is shown.

The assembling of the plastic-scintillator sheets used as ΔE_p-detectors or as an anticoincidence for the lead-glass counters is the same. Only the cross dimensions of the sheet and their thickness change. The thickness is 1 or 3 mm for ΔE_p and 10 mm for the anticoincidence. In fig.51 is presented a typical scheme. The light emitted by the plastic sheet is collected by two

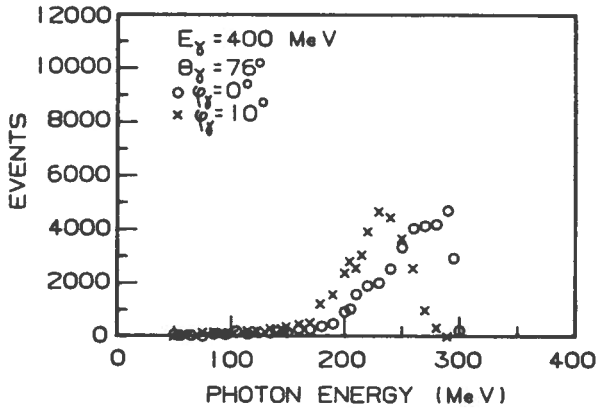

Fig.39 Result of a Monte-Carlo simulation for the photon energy distribution relative to the incident photon energy Eγ = 400 MeV, the azimuthal angles $\varphi_\gamma = 0^0$ and $10^0$and $\vartheta_\gamma = 76^0$

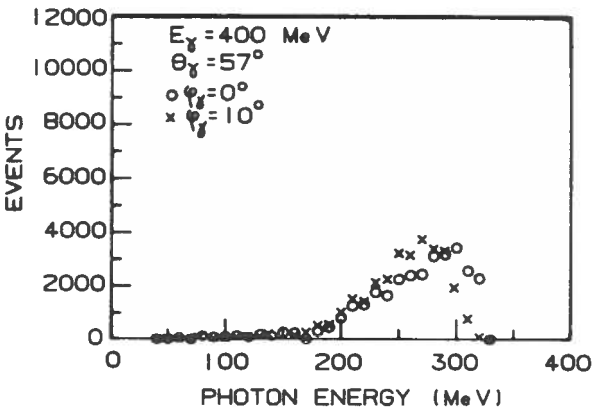

Fig.40 The same as fig.39 for $\vartheta_\gamma = 57^0$

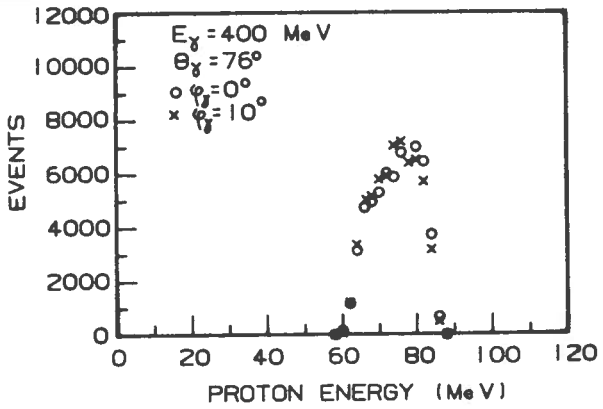

Fig.41 Result of a Monte-Carlo simulation for the proton energy distribution relative to the azimuthal angles $\varphi_\gamma = 0^0$ and 10^0, the incident photon energy $E_\gamma = 400$ MeV and $\vartheta_\gamma = 76^0$

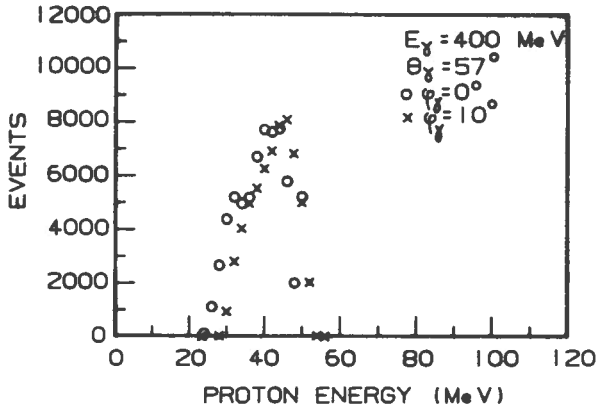

Fig.42 The same as fig.41 for $E_\gamma = 400$ MeV and $\vartheta_\gamma = 57^0$

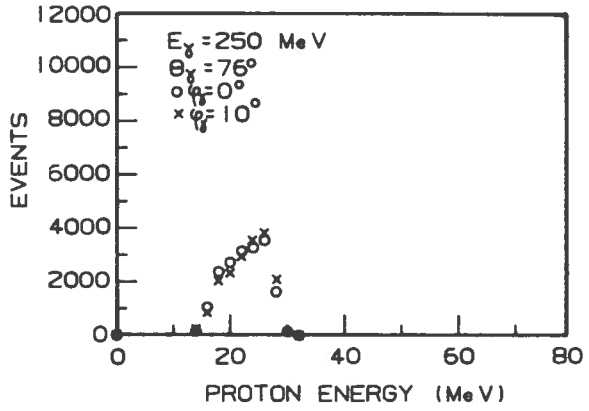

Fig.43 The same as fig.41 for $E_\gamma = 250$ MeV and $\vartheta_\gamma = 76^0$

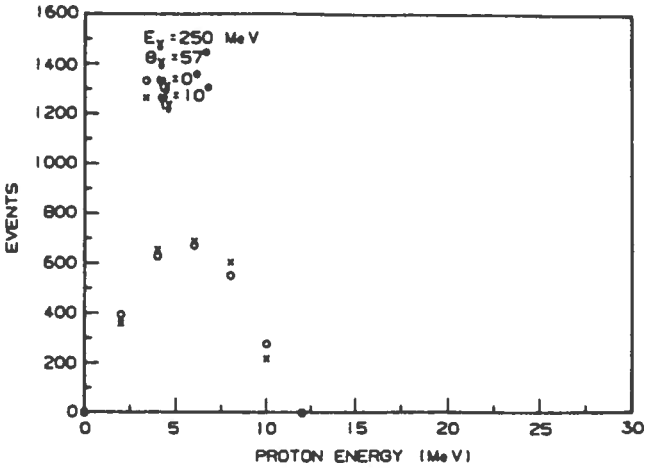

Fig.44 The same as fig.41 for $E_\gamma = 250$ MeV and $\vartheta_\gamma = 57^0$

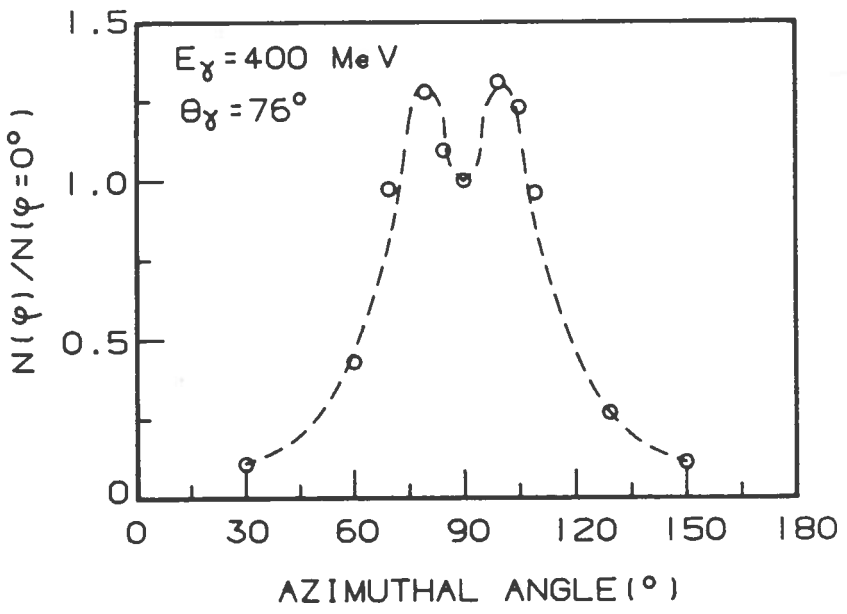

Fig.45 Result of a Monte-Carlo simulation for the number of events as a function of the azimuthal angle relative to the incident photon energy $E_\gamma = 400$ MeV and $\vartheta_\gamma = 76^0$

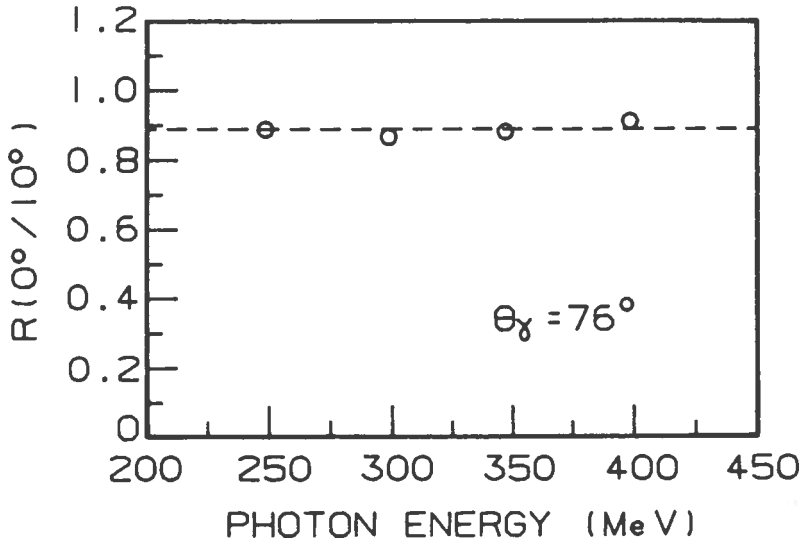

Fig.46 Result of a Monte-Carlo simulation for the ratio between the number of events at $\varphi_\gamma = 0^0$ and at $\varphi_\gamma = 10^0$as a function of the incoming photon energy and for $\vartheta_\gamma = 76^0$

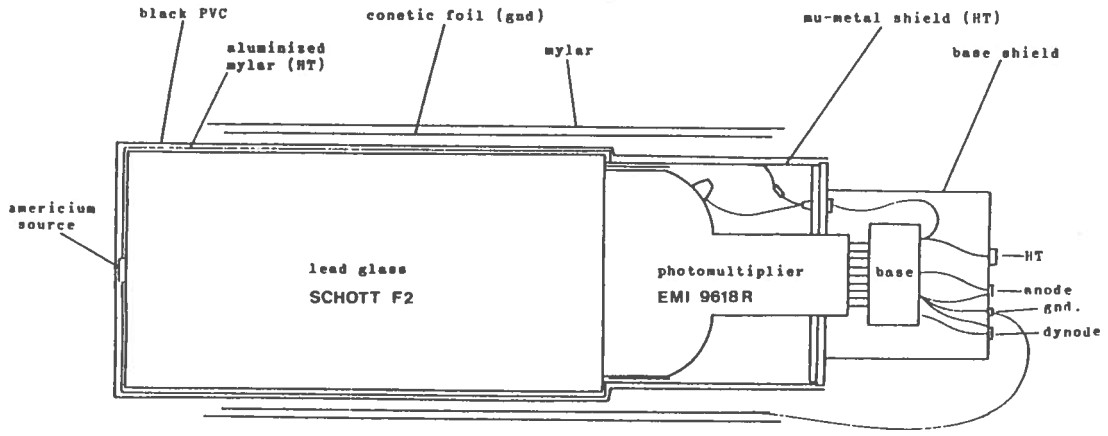

Fig.47 Layout of the lead-glass detector

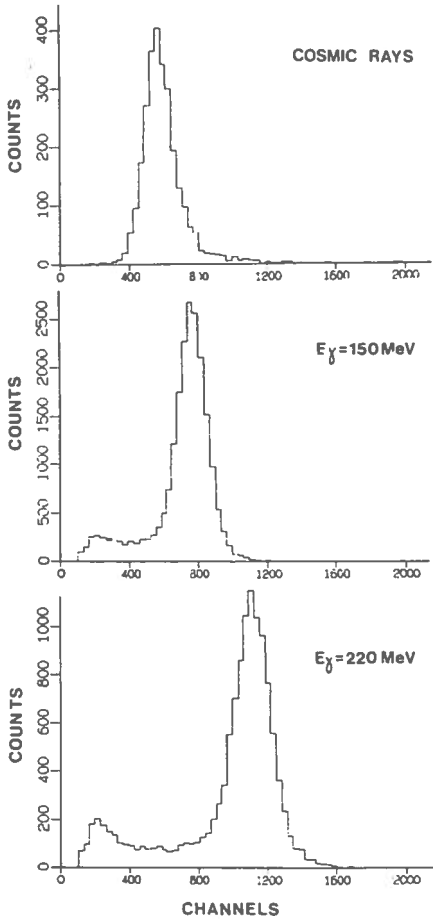

Fig.48 Lead-glass detector response to the cosmic rays and to 150 and 200 MeV monochromatic photons

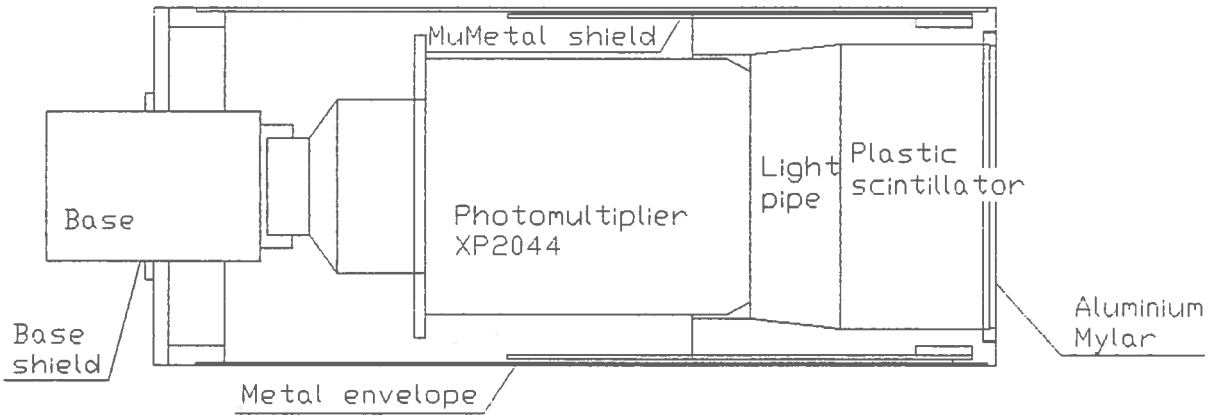

Fig.49 Layout of the plastic-scintillator detector

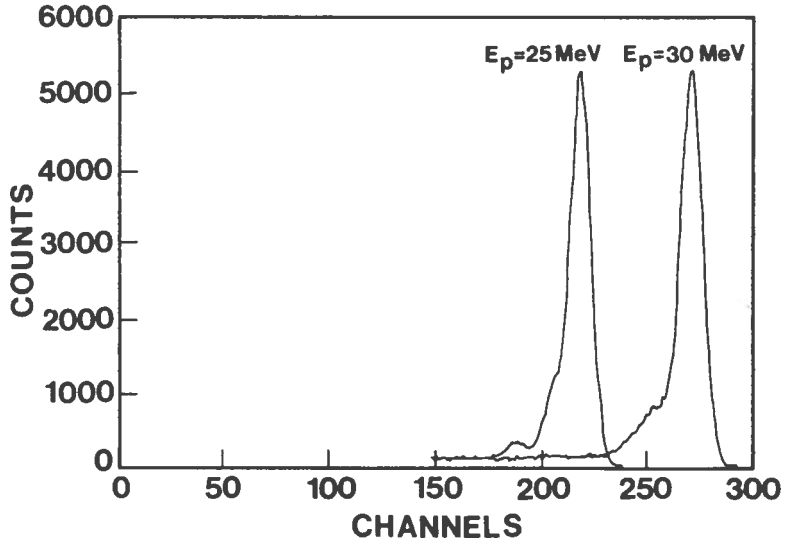

Fig.50 Plastic-scintillator detector response to 25 and 30 MeV monochromatic protons obtained by the proton scattering from ^{12}C at $\varphi = 15^{o}$

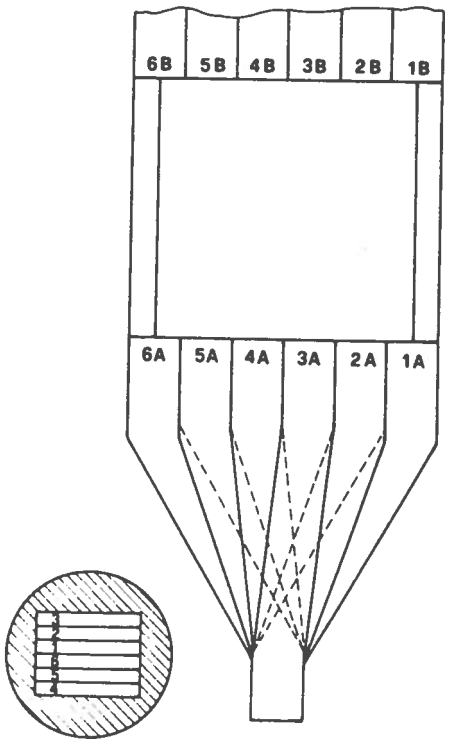

Fig.51 Layout of the plastic-scintillator detector

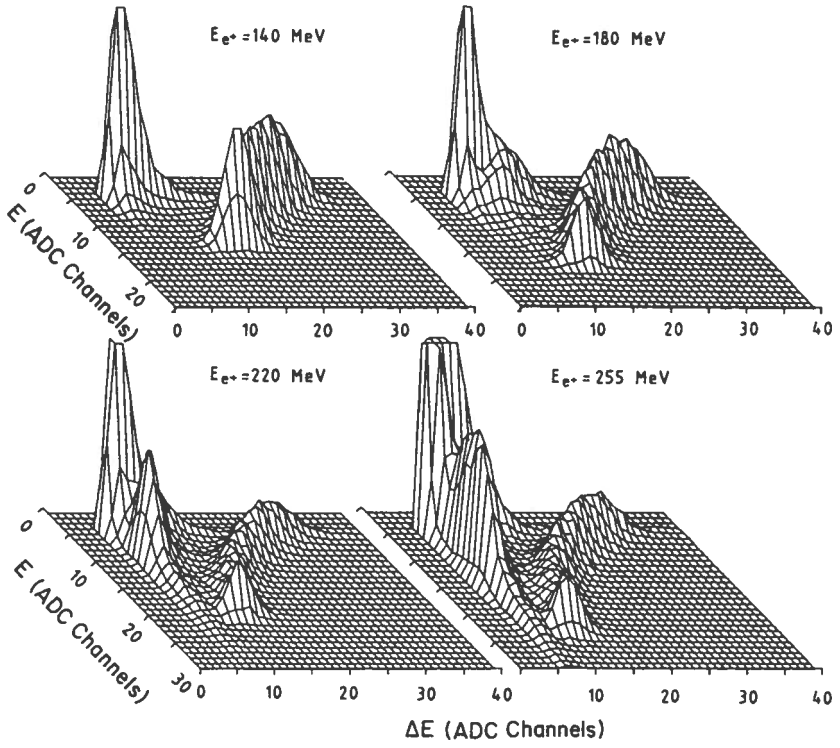

Fig.52 Typical ΔE vs E plots for a proton telescope

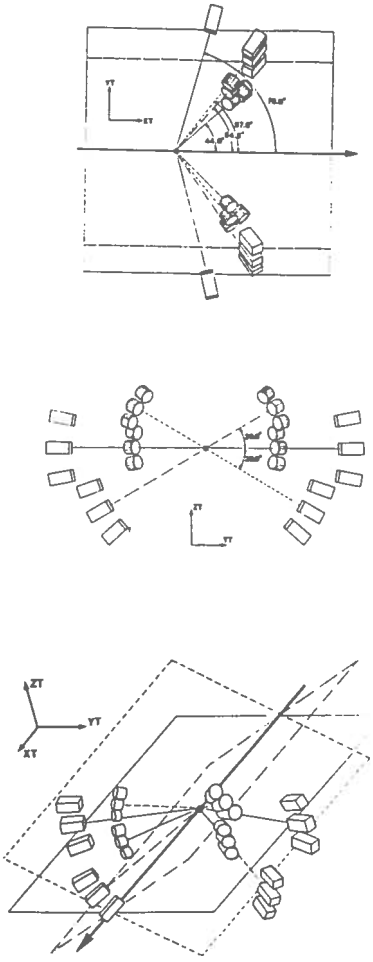

Fig.53 Display of the detector configuration for the simultaneous measurement of the differential cross section at $\vartheta^{cms} = 90^{o}$ and $\vartheta^{cms} = 70^{o}$

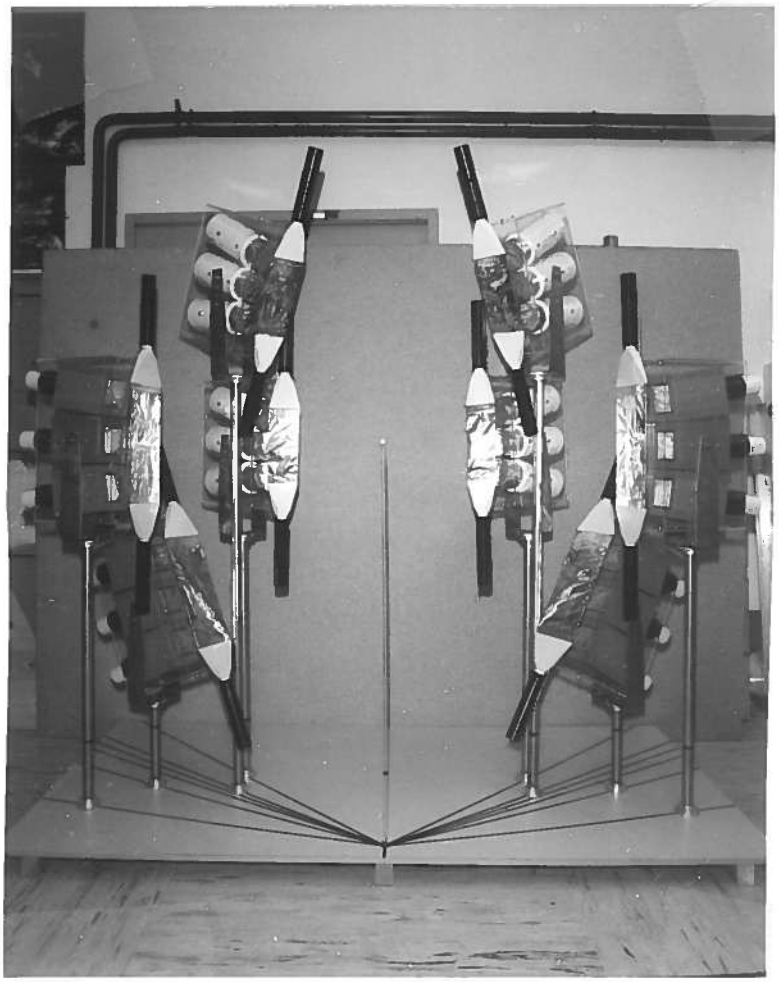

Fig.54 Model for the arrangement of all the detectors in the configuration of fig.53

photomultipliers through light-pipes which are divided in sectors in order to increase the light collection efficiency. A typical ΔE-E plot capability obtainable with this kind of telescope is presented in fig.52. The figure shows that the mass discrimination capability allows to distinguish unambiguously the protons from the other particles.

The 6 lead-glass detectors (and the 6 plastic-scintillator ones) are divided into two groups of 3 counters each. The three counters of each group are located at the same ϑ but at different φ so that between two adjacent detectors $\Delta\varphi = 10^o$. Moreover the two groups are located at $\Delta\varphi = 180^o$ one another. In fig.53 the configuration of the detectors is displayed in the case of a simultaneous measurement of the cross section at $\vartheta^{cms} = 90^o$ and $\vartheta^{cms} = 70^o$.

Finally in fig.54 is presented a mock-up built in order to show the arrangement of all the detectors in the case of the configuration of fig.53.

The position of adjacent detectors in each group at a distance of $\Delta\varphi = 10^o$ has been decided in order to make possible the coincidence between a proton and a photon detector "in plane" and "out of plane". In this way it will be possible, as already discussed at the end of section 3, to measure at the same time the total proton spectrum, due to the scattering and to the π^o-production and the contribution of the π^o-production alone.

The front-end of the data acquisition system is built with CAMAC modules. They are mainly from standard industrial production but someone is developed at Frascati National Laboratory.

The CAMAC crates and the modules are controlled by a peripherical intelligent system (E-6 by Eltec, 68030 CPU) in a VME crate.

The data collection and the preliminary analysis will be done by the E-6 processor. For further analysis and for the mass-memory stocking the data will be dispatched through Ethernet to a VAX system. The acquisition program running on the E-6 processor is MECDAS developed in the Nuclear Physics Institute of the Mainz University[13]. The analysis program running on the VAX system is GOOSY developed at the GSI Laboratory in Darmstadt[14].

A third processor (MAC IIX) will be connected to the VME crate by a MICRON card and a MACVEE module. In the MAC IIX will run two programs, developed at Genova University and at LNF. The first one controls automatically the gain of the photomultipliers, the second is responsible for the general set-up of the remote controlled CAMAC-ECL modules.

In fig.55 is reported a general schematic diagram of the acquisition system. In figs.56a, b and c are reported in some detail the electronic modules connection for the front-end, the logic and the services.

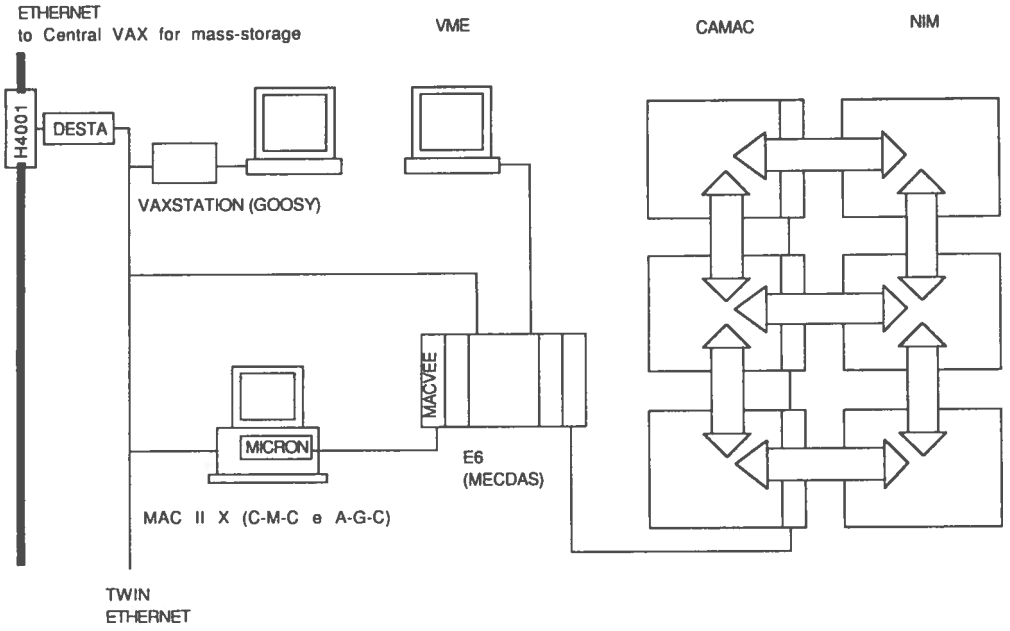

Fig. 55 Schematic diagram of the acquisition system

5. CONCLUSIONS

We will summarize now the most important characteristics of this project of experiment. The use of monochromatic tagged photons, the close definition of kinematics and the simultaneous measurement of the coincidences "in plane" and "out of plane" will produce a complete rejection of the background in the measurement of the photon scattering differential cross section.
Moreover the use of tagged photons will give the possibility to know the intensity of the employed photons with a good precision and to do a simultaneous measurement in the whole energy region of the Δ-resonance.
The counting rate and consequently the statistical accuracy will depend obviously on the photon intensity and on the tagging system characteristics. They have been evaluated starting from the formula

$$C = N_\gamma (E_\gamma) \frac{d\sigma (E_\gamma, \vartheta)}{d\Omega} \Delta\Omega \, N_H \, \varepsilon_t$$

where

$N_\gamma (E_\gamma)$ number of photons per second in $\Delta E_\gamma / E_\gamma = 0.05$

$\frac{d\sigma (E_\gamma, \vartheta)}{d\Omega} \cong 0.2$ μb/sr expected average value

$\Delta\Omega = 42$ msr total solid angle
$N_H = 2.5 \; 10^{23}$ atoms/cm^2 for a liquid Hydrogen target 6 cm long
ε_t tagging efficiency

In the evaluation we have assumed for Nγ (Eγ) and ε_t the expected values of the JET-TARGET facility at Frascati National Laboratory[15] and of the MAMIB facility at Mainz University[16].

The characteristics of the two photon beams and the results of the evaluation are summarized in Table 4.

TABLE 4

Facility	Nγ (Eγ) photons/sec	ε_t	C (Eγ) events/sec	ΔT hours	C_{tot}	$\Delta C_{tot}/C_{tot}$
JET-TARGET	$2.5 \; 10^5$	0.8	$4.2 \; 10^{-4}$	264	400	0.05
MAMIB	$5 \; 10^6$	0.5	$5.3 \; 10^{-3}$	132	2500	0.02

where ΔT is the measure time, C_{tot} the total number of events and $\Delta C_{tot}/C_{tot}$ the statistical accuracy.

The values of the first colum are obtained taking

$$N_\gamma (E_\gamma) = 5 \; 10^6 \frac{dE_\gamma}{E_\gamma} \frac{\text{photons}}{\text{sec}}$$ for the JET-TARGET

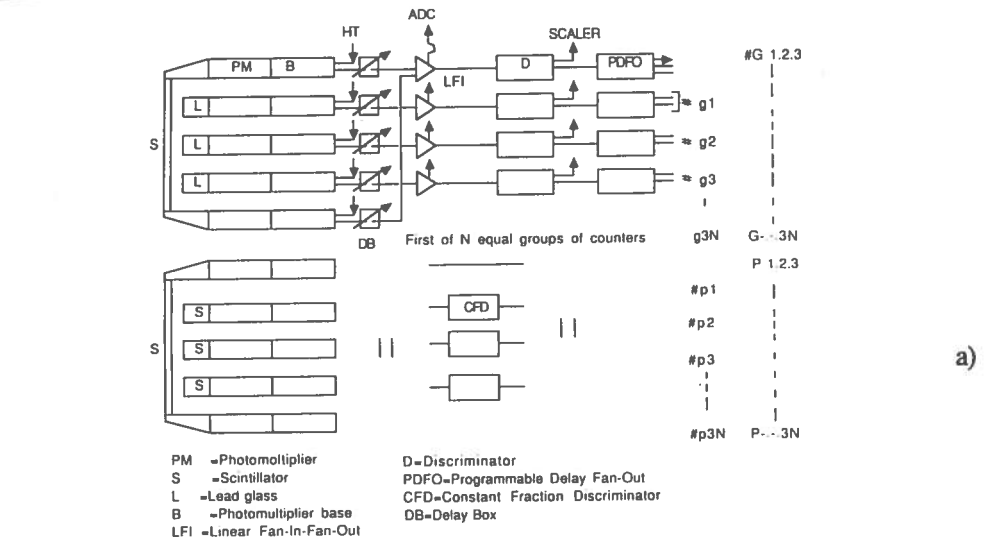

a)

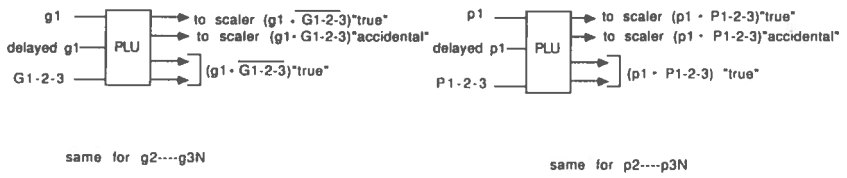

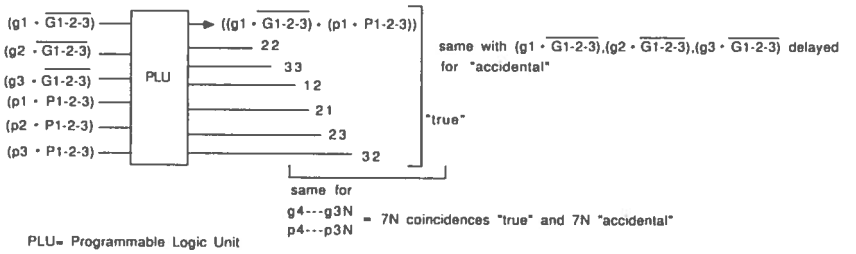

b)

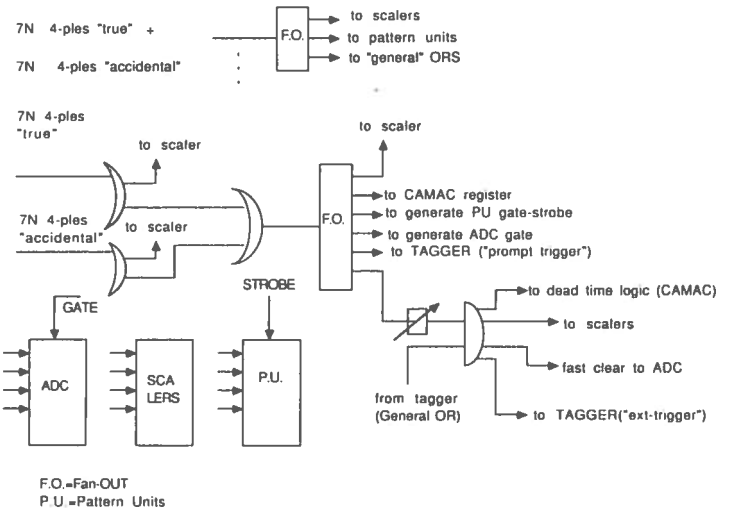

c)

Fig.56 Block-scheme of a) - the electronic system, b) - the logic and c) - the services

$N_\gamma = 10^6 \frac{\text{photons}}{\text{sec}}$ in $\Delta E_\gamma = 4\,\text{MeV}$ for the MAMIB facility

As a conclusion we can say that with the apparatus described above it is possible to do a measurement of the p (γ, γ) reaction differential cross section with a statistical accuracy of 2% and a comparable systematic error.

REFERENCES

1 a) R.Leicht, M.Hammen, K.P.Schelhaas and B.Ziegler, Nuclear Physics A362 (1981) 111

b) M.Sanzone-Arenhovel, K.P.Schelhaas and B.Zieglier, Intermediate Energy Nuclear Physics, World Scientific Singapore 1982 pag.291

c) K.P.Schelhaas, J.M.Henneberg, M.Sanzone-Arenhovel, N.Wieloch-Laufenberg, U.Zurmuhl, B.Ziegler, M.Schumacher and F.Wolf, Nuclear Physics A489 (1988) 189

2 a) E.Hayward and B.Ziegler, Nuclear Physics A414 (1984) 333

b) E.J.Austin, E.C.Booth, E.K.McIntyre, J.P.Miller, B.L.Roberts and D.A.Whitehouse, Physical Review Letters 57 (1986) 972

c) E.J.Austin, E.C.Booth, D.Delli Carpini, K.P.Gall, E.K.McIntyre, J.P.Miller, D.Warner, D.A.Whitehouse and G.Dodson, Physical Review Letters 61 (1988) 1922

3 a) J.Vesper, N.Ohtsuka, L.Tiator and D.Drechsel, Physics Letters 159B (1985) 232

b) J.Vesper, D.Drechsel and N.Ohtsuka, Nuclear Physics A466 (1987) 652

4 a) H.Koch, E.J.Moniz and N.Ohtsuka, Annal Physics 154 (1984) 99

b) J.H.Koch, private communication

5 H.Arenhovel, M.Weyrauch and P.C.Reinhard, Physics Letters 155B (1985) 22

6 a) H.Genzel, M.Jung, K.R.Rausch, R.Wedemeyer and H.J.Weyer, Lettere al Nuovo Cimento 4 (1972) 695

b) H.Genzel, M.Jung, R.Wedemeyer and H.J.Weyer, Zeitung Physik A279 (1976) 399

7 H.Genzel, P.Joos and W.Pfeil, Landolt Bornstein, New Series Group I, (1973) Vol.8. Edit.H.Schopper

8 M.Gell-Mann, M.L.Goldberger and W.E.Thirring, Physical Review 95 (1954) 1612

9 J.Ahrens, Nuclear Physics A446 (1985) 229 C

10 a) R.Koberle, Physical Review 166 (1968) 1558

b) W.Pfeil, H.Rollnik and S.Stankowski, Nuclear Physics B73 (1974) 166

c) D.M.Akhmedov and L.V.Fil'kov, Nuclear Physics B125 (1977) 530

d) I.Guiasu, C.Pompiniu and E.E.Radescu, Annals Physics 114 (1978) 296

e) G.Kolbel, Diplomarbeit Bonn University 1978

11 A.M.Boldin, V.I.Gol'danskii and I.L.Rozenthae, Kinematics of Nuclear Reactions, Pergamon Press 1961

12 C.Baglin + al, Phys.Letters B (1987) 85

13 K.W.Krigier, V.Kunde - Basic Features of MECDAS - KPH Mainz, August 89

14 H.G.Essel, T.Kroll, M.Richter, H.Sohlbach, W.Spreng - GOOSY, The Acquisition and Analysis System for Experimental Data - GSI Darmstadt

15 M.Albicocco + al, Report LNF-86/29(R) (1986)

16 Jahresbericht 1986-1987 - Institute fur Kernphysik - Universitat Mainz